Structural and Multidisciplinary Optimization (2025) 68:158
https://doi.org/10.1007/s00158-025-04102-y

RESEARCH PAPER

On the application of the multigrid method to topology optimization with orthotropic material with varying orientation

Jan Christoph Krüger[1] · **Benedikt Kriegesmann**[1]

Received: 4 March 2025 / Revised: 11 June 2025 / Accepted: 27 July 2025
© The Author(s) 2025

Abstract
Multigrid methods are known to show good performance for most topology optimization problems, but suffer from anisotropies. The main problems are caused by poor performance of the smoothing algorithms. This paper analyzes different standard and advanced smoothing algorithms using the local Fourier analysis with regard to orthotropic materials in the linear elasticity problem. The results are generalized to real problems and contrast-rich topology designs using numeric experiments. Based on the analyses, recommendations are given and a new spatial Jacobi smoothing algorithm is presented. The results are finally approved by a topology optimization example and a material orientation and topology optimization example.

Keywords Multigrid method · Topology optimization · Material orientation and topology optimization · Orthotropic material · Large scale

1 Introduction

Topology optimization has become a useful and widely accepted approach for computational design. While the first applications of topology optimization were mainly restricted to 2D problems with less than 10,000 voxel finite elements (Buhl et al. 2000; Hammer and Olhoff 2000), increasing computational resources and new algorithms led to a wider applicability of this method. A huge effort has been taken for the solution of linear systems of equations arising from the finite element method, since this part is responsible for the main computation time and memory demands. In the context of parallel computing and the use of high-performance clusters, domain decomposition methods help to distribute the computational load to several workers. By doing this, also medium sized 3D-problems were solved in the early topology optimization days (Borrvall and Petersson 2001; Mahdavi et al. 2006; Evgrafov et al. 2008). Other approaches focused on improving iterative Krylov subspace solvers, for example, by approximate reanalysis techniques (Amir et al. 2009) and recycling of parts (Wang et al. 2007; Amir and Sigmund 2011).

A huge increase in efficiency for solving linear systems of equations was achieved by the application of the multigrid method. Although this method has been known for many decades (see, e.g., Shaidurov (1995)) and it was early applied to topology optimization (Dreyer et al. 2000), it gained attention after the first educational paper by Amir et al. (2014). There, a Galerkin projection-based geometric multigrid method is used as a preconditioner for the conjugate gradient method. With this, it is possible to run topology optimization problems that have been called "large scale" in the early days on a simple laptop. Several publications followed, applying the multigrid method to open-source code (Aage et al. 2015), to giga-scale problems (Aage et al. 2017) and to shell structures (Träff et al. 2021). Others present highly efficient implementations exploiting the narrow band structure of the stiffness matrix (Liu et al. 2018) or using graphic processor units (Wu et al. 2016; Herrero-Pérez and Martínez Castejón 2021; Padhi et al. 2023).

Despite these achievements, there are still open challenges. Besides the problem of high-contrast designs, anisotropic behavior of the partial differential equation also leads to significantly reduced convergence rates of the multigrid

Responsible editor: Marco Montemurro

✉ Jan Christoph Krüger
jan.krueger@tuhh.de

Benedikt Kriegesmann
benedikt.kriegesman@tuhh.de

[1] Institute for Structural Mechanics in Lightweight Design, Hamburg University of Technology, Eißendorfer Straße 40, 21073 Hamburg, Germany

Published online: 21 August 2025

solution (Trottenberg et al. 2007). The (discretized) partial differential equation becomes anisotropic when using orthotropic materials or in the context of stretched finite elements. This effect usually does not occur in topology optimization since often the problem is solved on a voxel mesh with isotropic material (e.g., 3D printed steel). However, anisotropic problems also occur in reality.

Application of the simple multigrid approach presented in Amir et al. (2014) with the same settings (damping factor $\omega = 0.6$) to the same cantilever example but with carbon fiber-reinforced polymer (CFRP) as material leads to much worse performance. Figure 1a shows the numbers of required multigrid iterations for different fiber orientations at the initial design. The black curve corresponds to the CFRP problem, and the blue curve corresponds to the isotropic problem from Amir et al. (2014). For all orientations, the number of iterations sticks at approximately 1000, which is also the maximum allowed number of iterations.

To retrieve acceptable performance for all orientations, the damping factor must be significantly reduced to $\omega = 0.3$. As shown in Fig. 1b , this reduces the number of iterations to approximately 50. However, the iteration number is still significantly higher than the number of iterations required for isotropic materials.

For the case of stretched finite elements, Peetz and Elbanna (2021) show that using algebraic multigrid reduces the number of solver iterations. However, they conclude that the additional effort for setting up the algebraic operators is much higher than the gain in 3D. On the other hand, already early publications showed that plane-smoothing (Oosterlee 1997) or semi-coarsening (Morano et al. 1998) are very effective for a priori known constant anisotropies. However, the assumption of a priori known constant anisotropies is not valid in practice.

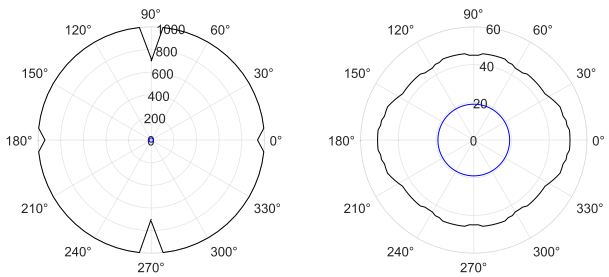

(a) CFRP, $\omega = 0.6$ (b) CFRP, $\omega = 0.3$

Fig. 1 Number of iterations to solve a linear equation using multigrid preconditioned conjugate gradients with Jacobi smoothing and a relative residual of less than 10^{-10}. The radius corresponds to the number of iterations, the angle represents the rotation angle of the material. The blue plot corresponds to an isotropic material with Poisson's ratio 0.3. The black plot corresponds to a carbon fiber reinforced polymer

For example, orthotropic mechanical properties occur in natural organic material such as wood. A topology optimization of wooden structures is, for example, presented in Ma et al. (2021) and de Vito et al. (2023). In general, the orientation is not constant over the domain since effects of branches and unsteady growth lead to spatially varying fiber orientations. Additionally, the two weak directions are oriented into the radial and tangential directions of the trunk (Thibaut et al. 2001; Da Silva and Kyriakides 2007) instead of the Cartesian coordinate system. However, the orientation is given and cannot be (spatially) influenced by the manufacturing process. Hence, the non-constant material orientations are known a priori.

The special case of transversal isotropic material occurs in the context of composite materials and 3D printing based on filaments. There, the material orientations are chosen by the designer. Whereas classic laminates only allow small variations in material orientations, there are already some endless fiber 3D printers based on the fused filament fabrication principle. Additionally, special multi-axial 3D printers allow material orientations in all three dimensions (Kipping and Schüppstuhl 2023; Steltner et al. 2024). Hence, the spatial material orientation is considered as an additional design variable in Lund (2017), Lee et al. (2018), Jantos et al. (2020), and Schmidt et al. (2020), which can also be parameterized using splines (Montemurro et al. 2024). This leads to non-constant and not a priori known anisotropies.

The current contribution aims at giving a decision basis about which multigrid components (especially which smoother) to choose for which type of anisotropic problem. Therefore, different basic approaches are analyzed and benchmarked. Additionally, a new method is proposed to improve the convergence speed. The paper is organized as follows: First, the general multigrid principle is shown. Afterwards, different standard approaches are analyzed using the local Fourier analysis and compared considering computational cost. In the following, these approaches are further investigated by numerical experiments at different (topology optimized) designs. A new approach called spatial Jacobi smoothing is proposed and compared to the previous methods. In the end, some of the methods are applied to different examples of material orientation and topology optimization as well as topology optimization of a wood structure.

2 Solution of the linear equations

The focus of the current publication is to solve the general equation

$$\boldsymbol{K} \cdot \boldsymbol{u} = \boldsymbol{f}, \tag{1}$$

where $\boldsymbol{K}$ is an arbitrary symmetric and sparse matrix originating from a discretized partial differential equation, $\boldsymbol{u}$ is the state and $\boldsymbol{f}$ is an arbitrary vector.

Using a direct solver, the solution of (1) is found after approximately $\mathcal{O}(n^{3/2})$ operations, where n represents the number of finite elements (Davis 2006). While this is a good performance for small models, the computation time and memory demands become infeasible for large models.

In contrast, iterative methods such as the conjugate gradient method (Hestenes and Stiefel 1952) and the generalized minimal residual method (GMRES) (Saad and Schultz 1986) are mainly based on vector–matrix products. The memory requirements are very low, while the computation time depends on the number of iterations. It is known that the required number of iterations for reaching a given tolerance depends on the condition number, which can be improved by a preconditioner. One very efficient preconditioner is the multigrid method described in Stüben and Trottenberg (1982), Fulton et al. (1986), Wesseling (1992), Briggs et al. (2000), and Trottenberg et al. (2007).

2.1 General multigrid procedure

The basic concept of the multigrid method is to combine the advantages of basic iterative methods with a solution on a coarse mesh. Simple iterative solvers/smoothers, such as the damped Jacobi method are known to reduce high-frequency error components very effectively while low-frequency components remain. In difference, the solution on a coarse mesh only removes low-frequency errors since high-frequency errors are not represented there. Combining both components leads to the multigrid method, where both, low- and high- frequency errors are removed. It has been shown that the multigrid solver only requires $\mathcal{O}(n)$ operations for the Poisson equation if all components are chosen properly (Trottenberg et al. 2007) and hence, it is much more effective than direct solvers for large problems. However, if the components are not chosen properly, the convergence rate suffers. Using the multigrid method as a preconditioner for another iterative method, this issue is reduced.

The overall framework of using multigrid as preconditioner is depicted in Fig. 2. Using the V-cycle, the procedure starts with an initial guess of the solution u_1 (e.g., a zero vector) and the right-hand side f. Inside the outer solver function, the residual is computed. This residual is forwarded to the multigrid preconditioner. On the finest level, a smoothing operator $smooth(\boldsymbol{f}_1)$ (e.g., Jacobi method) is applied and the resulting residual $\boldsymbol{r}_1$ is restricted to a coarser mesh using the restriction operator $\boldsymbol{R}$. The same procedure is repeated on the following meshes until the coarsest mesh is reached (mesh 3 in the figure). On the coarsest mesh, the system of equations is solved exactly (e.g., using direct methods or another iterative solver). Note that the size of the problem is significantly reduced on the coarsest mesh. In the following, the coarse grid solution is prolonged to a finer mesh using a prolongation operator $\boldsymbol{P}$. The result is smoothed on the fine mesh and again prolonged to a finer mesh. This procedure is repeated until the finest mesh is reached. The result of the finest mesh is then transferred to the outer iterative solver (e.g., conjugate gradient). Using the W-cycle (also shown in Fig. 2), the framework is similar. However, the cycle includes additional restrictions after a prolongation.

2.2 Local Fourier analysis (LFA)

The local Fourier analysis is a simple analytic tool to compute the local smoothing properties of different basic iterative methods (such as Jacobi smoothing). The basic concept of the local Fourier analysis is to consider a discretized partial differential equation with constant coefficients (e.g., material properties) and assume an infinite grid (i.e., no effect of boundary conditions) with constant spacing h. Using eigenfunctions, the amplification of different components of the residuum caused by the smoothing operator is computed analytically. Since only local effects are studied, the assumption of

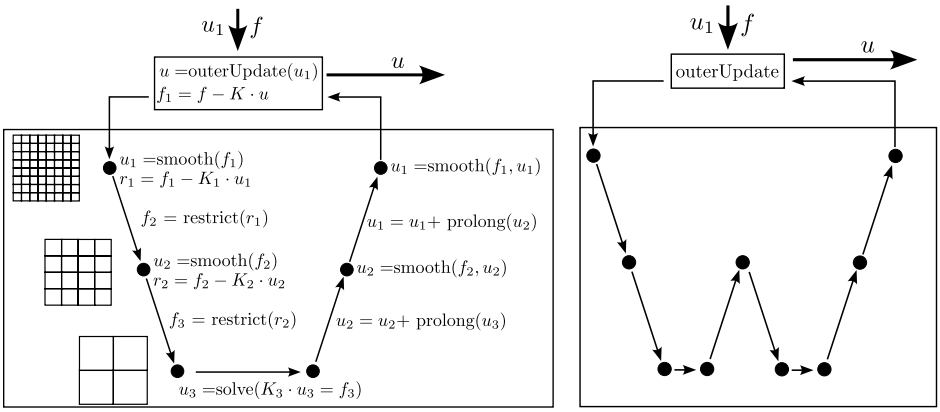

Fig. 2 Framework of a multigrid preconditioned iterative solver. The indices represent the corresponding grid level. Left: V-Cycle, right: W-Cycle

(locally) constant coefficients is also fulfilled for smoothly varying coefficients. A detailed introduction is found in Wienands and Joppich (2004) and Trottenberg et al. (2007). The general error of the state $\boldsymbol{v} = \boldsymbol{u} - \boldsymbol{u}_{true}$ at the position $\boldsymbol{x} + \Delta\boldsymbol{x}$ is represented by an exponential series $\boldsymbol{v}(\boldsymbol{x} + \Delta\boldsymbol{x}) = \sum_j \hat{\boldsymbol{v}}_j(\boldsymbol{x}) e^{i\boldsymbol{\Theta}_j^T \Delta\boldsymbol{x}/h}$ with the grid spacing h and the continuous vector valued error-frequency

$$\boldsymbol{\Theta}_j = \begin{pmatrix} \Theta_{x,j} \\ \Theta_{y,j} \\ \Theta_{z,j} \end{pmatrix} \in \begin{pmatrix} [-\pi, \pi] \\ [-\pi, \pi] \\ [-\pi, \pi] \end{pmatrix} \quad . \tag{2}$$

During the smoothing process, the error of the state is modified by the smoothing operator $smooth(\boldsymbol{v})$. In many cases (e.g., Jacobi), smoothing does not cause any error mixing. This means that smoothing of an error component $\hat{\boldsymbol{v}}_j e^{i\boldsymbol{\Theta}_j^T \Delta\boldsymbol{x}/h}$ leads to an error with the same frequency but a different magnitude. Using local Fourier analysis, for every allowed frequency $\boldsymbol{\Theta}$ the corresponding amplification matrix function $\boldsymbol{S}_h(\boldsymbol{\Theta})$ is computed, such that

$$smooth(\hat{\boldsymbol{v}}_j e^{i\boldsymbol{\Theta}_j^T \Delta\boldsymbol{x}/h}) = \boldsymbol{S}_h(\boldsymbol{\Theta}_j) \hat{\boldsymbol{v}}_j e^{i\boldsymbol{\Theta}_j^T \Delta\boldsymbol{x}/h} \tag{3}$$

and following

$$smooth(\boldsymbol{v}) = \sum_j \boldsymbol{S}_h(\boldsymbol{\Theta}_j) \hat{\boldsymbol{v}}_j e^{i\boldsymbol{\Theta}_j^T \Delta\boldsymbol{x}/h} \quad . \tag{4}$$

For background to the practical computation, the reader is referred to Trottenberg et al. (2007). In the context of the multigrid method, low-frequency errors are corrected by the coarse grid operations, while high-frequency errors must be corrected by the smoothing algorithm. The error is classified as low-frequency if $\boldsymbol{\Theta} \in \begin{pmatrix} [-\frac{\pi}{2}, \frac{\pi}{2}] \\ [-\frac{\pi}{2}, \frac{\pi}{2}] \\ [-\frac{\pi}{2}, \frac{\pi}{2}] \end{pmatrix}$, which means that the wavelength of the error is higher than one element size and hence, seen on the coarse grid. The smoothing factor is then defined as

$$\mu_{loc} = \sup_{\boldsymbol{\Theta}} (\| \rho(\boldsymbol{S}_h(\boldsymbol{\Theta})) \| \, : \, \Theta \in [-\pi, -\frac{\pi}{2}] \cup [\frac{\pi}{2}, \pi]) \tag{5}$$

with $\rho(\boldsymbol{S}_h(\boldsymbol{\Theta}))$ being the spectral radius of the matrix $\boldsymbol{S}_h(\boldsymbol{\Theta})$. In the following, $\rho(\boldsymbol{S}_h(\boldsymbol{\Theta}))$ is called the amplification factor, since it represents how much an error with the frequencies $\boldsymbol{\Theta}$ is amplified. Since the high-frequency error should be reduced, the amplification factor must be lower than 1 for all high frequencies, and hence, the smoothing factor μ_{loc} must be lower than 1.

Application of the local Fourier analysis to the Jacobi method with the standard isotropic material gives the amplification factors shown in Fig. 3. There, the frequency in the z-direction is set to zero, while the amplification factor is given for different frequencies in the x- and y-directions. The white part of the surface plot indicates the low-frequency domain and the green part indicates the high-frequency domain. For all frequencies, the amplification factor stays below one, meaning that the Jacobi method is also stable as a standalone solver. In general, the amplification factors are lower in the relevant high-frequency domain. There, the worst amplification factor is found at the border to the low frequency domain with $\mu_{loc} \approx 0.75$.

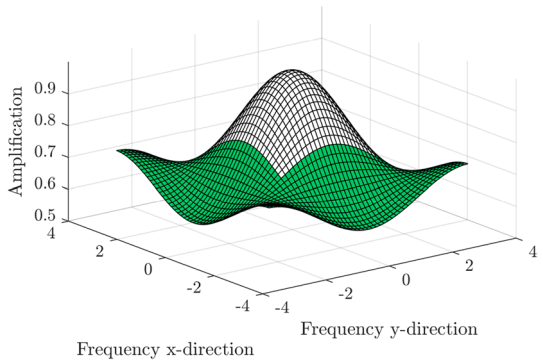

Fig. 3 Amplification factors from the local Fourier analysis of Jacobi smoothing with $\omega = 0.5$ for isotropic material. The x- and y-axis represent the frequency of the error of the state in x-/y-direction. The z-axis represents the corresponding amplification factor. For visualization reasons, the error frequency in z-direction is set to 0

3 Theoretic analysis of common smoothing methods for orthotropic materials

Besides the Jacobi method, there are many other common smoothing algorithms, such as the Gauß-Seidel method, line-smoothers and plane-smoothers. The Gauß-Seidel method is known to be more robust and shows better smoothing properties than the Jacobi method. However, it is known to show similar behavior to the Jacobi method for anisotropic partial differential equations. Alternatively, line-smoothers and plane smoothers are recommended for anisotropic problems in literature, but have not been tested for the special case of topology optimization and non-constant orientations. In general, all alternatives to the Jacobi method are more computational costly and complex to implement efficiently. Hence, a fair comparison does not only include the required number of solver iterations, but also the (theoretical) computational effort to apply one smoothing step as well as the parallelizability. These methods are shortly explained and analyzed using local Fourier analysis. Afterwards, the methods are compared regarding smoothing properties for different material orientations and computational cost. As exemplary material, Balsa wood with the mechanical

properties shown in Appendix D.2 is considered, since it is a commonly used wood and shows highly orthotropic behavior. However, the results can be generalized to other materials with comparable stiffness ratios and transversal isotropic materials, such as carbon fiber reinforced polymers.

In the current contribution, the (spatially varying) material orientation of the orthotropic material is described by the cardan angles as depicted in Fig. 4. In the original coordinate system, the orthotropic material has its highest stiffness in the X-direction and the lowest stiffness in the Y-direction. The first rotation η acts around the X-axis, the second rotation φ acts around the new z-axis and the third rotation θ acts around the new y-axis. Note that the specific description of the material orientation is only required for practical generation of the material tensor. The performance of the multigrid components is only influenced by the resulting discretized partial differential equation i.e., the (tangential) stiffness matrix, and not by the specific representation of the material orientation.

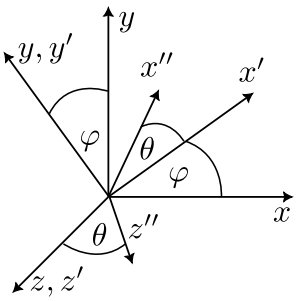

Fig. 4 Rotations of the transversal isotropic material. For the orthotropic material, an additional rotation η around the x-axis is done before. In the initial system, the material has the highest stiffness in x-direction and the lowest stiffness in the y-direction

3.1 Jacobi method

Due to its simplicity and low computational cost, the damped Jacobi method is often used as a smoother for the multigrid method (Amir et al. 2014; Aage et al. 2015; Peetz and Elbanna 2021). The response update $\boldsymbol{u}_{i+1}$ is computed by

$$\boldsymbol{u}_{i+1} = \boldsymbol{u}_i + \omega \boldsymbol{D}^{-1} \cdot \left(\boldsymbol{f} - \boldsymbol{K}\boldsymbol{u}_i\right), \tag{6}$$

where $\boldsymbol{D}$ represents the diagonal of the system matrix $\boldsymbol{K}$. As discussed in the introduction, the Jacobi method substantially suffers from orthotropic material behavior. The reason for the poor performance in the context of orthotropic material is further analyzed using local Fourier analysis (LFA).

Considering only 0° orientations and using the damping factor $\omega = 0.5$, the amplification factors depicted in Fig. 5a are found. Compared to the example with isotropic material (Fig. 3), the amplification factors are much higher. Especially the peaks for high frequencies in the x-direction indicate that the method is unstable. However, also in y-direction, the amplification factor is stuck slightly below 1. When using $\omega = 0.3$ instead, the amplification shown in Fig. 5b is observed. The previous unstable regions now show good performance with amplification factors below 0.9. However, the smoothing in the y-direction gets even worse with $\mu_{loc} \approx 0.98$. Hence, it is crucial to choose an appropriate damping factor to obtain a stable method with acceptable smoothing properties.

3.2 Decoupled point-Gauß-Seidel smoothers/ successive overrelaxation

The decoupled pointwise successive overrelaxation (SOR) is very similar to the damped Jacobi method. However, it

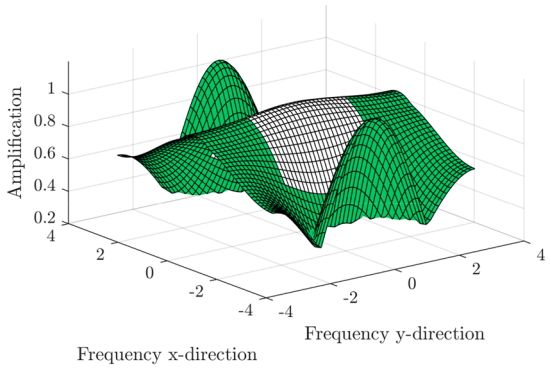

(a) $\omega = 0.5$

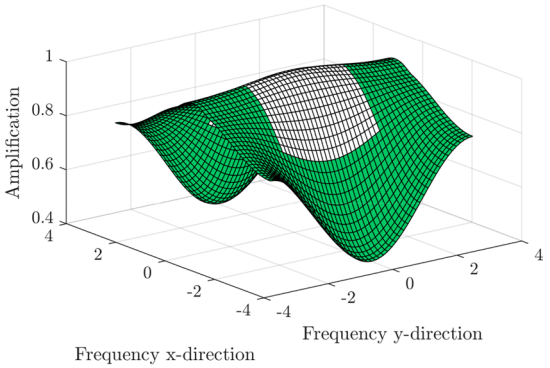

(b) $\omega = 0.3$

Fig. 5 Amplification factors from the local Fourier analysis of Jacobi smoothing for Balsa wood. The x- and y-axis represent the frequency of the error of the state in x-/y-direction. The z-axis represents the corresponding amplification factor. For visualization reasons, the frequency in z-direction is set to 0

solves a triangular instead of a diagonal system of equations. The state update reads

$$\boldsymbol{u}_{i+1} = \boldsymbol{u}_i + \left(\boldsymbol{L} + \frac{1}{\omega}\boldsymbol{D}\right)^{-1} \cdot \left(\boldsymbol{f} - \boldsymbol{K}\boldsymbol{u}_i\right) \tag{7}$$

with the strict lower triangular part $\boldsymbol{L}$ of the system matrix $\boldsymbol{K}$. The Gauß-Seidel method is the special case when using $\omega = 1$, whereas the method is called successive overrelaxation for $\omega > 1$. The smoothing properties depend on the node numbering of the finite element mesh. For a structured mesh, there are two major numbering groups: lexicographic numbering and the multicolor numbering. Similar numberings are also found for unstructured meshes. In the lexicographic numbering, the nodes are numbered linewise, such that neighboring nodes have following numbers (see Fig. 6a). If a line is finished, the first node of the next line has the following number. In difference, the multicolor numbering sorts the nodes into different color groups (see Fig. 6b). The groups are defined such that neighboring nodes belong to different colors. The node numbers are counted for each color separately. In Fig. 6b , black nodes have the numbers 1–9, red nodes the numbers 10–15, green nodes the numbers 16–21 and blue nodes the numbers 22–25. Using the multicolor numbering, the smoothing algorithm can be implemented in parallel without high implementation effort. A simple parallel formulation is explained in Appendix A. In difference, the lexicographic version is difficult to parallelize.

Applying the local Fourier analysis to the lexicographic Gauß-Seidel method for linear elasticity with Balsa wood (same orientation as before), the amplification factors shown in Fig. 7 are found. As for the Jacobi method, the amplification factor is stuck slightly below 1 in the y-direction, while good smoothing properties are obtained in the x-direction. However, no stability issues occur, and the absolute values are significantly better, leading to an overall smoothing factor $\mu_{loc} \approx 0.9$ instead of 0.98.

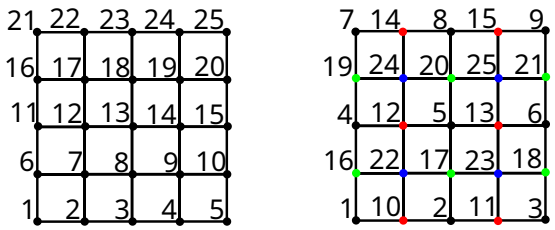

(a) Lexicographic numbering. (b) Multicolor numbering.

Fig. 6 Different node numbering schemes for the successive overrelaxation

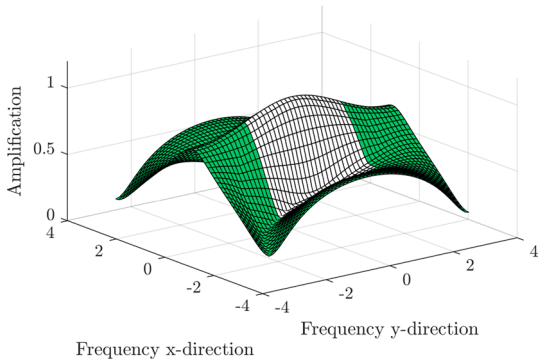

Fig. 7 Amplification factors from the local Fourier analysis of lexicographic Gauß-Seidel smoothing for Balsa wood. The x- and y-axis represent the frequency of the error of the state in x-/y-direction. The z-axis represents the corresponding amplification factor. For visualization reasons, the frequency in z-direction is set to 0

3.3 Coupled point successive overrelaxation

The coupled pointwise successive overrelaxation is similar to the decoupled successive overrelaxation. Again, the status update reads

$$\boldsymbol{u}_{i+1} = \boldsymbol{u}_i + \left(\boldsymbol{L}_p + \frac{1}{\omega}\boldsymbol{D}_p\right)^{-1} \cdot \left(\boldsymbol{f} - \boldsymbol{K}\boldsymbol{u}_i\right) \quad , \tag{8}$$

however here, the matrix $\boldsymbol{D}_p$ is a block diagonal matrix that contains couplings between different degrees of freedom of the same node. The lower triangular matrix $\boldsymbol{L}$ is modified such that $\boldsymbol{K} = \boldsymbol{L}_p + \boldsymbol{D}_p + \boldsymbol{L}_p^T$. If all rotations are set to 0, no couplings occur between the degrees of freedom of the same node, and hence, the coupled successive overrelaxation is equal to the decoupled version. Similar to the decoupled SOR method, the smoothing properties depend on the node numbering scheme. However, due to the block diagonal structure of $\boldsymbol{D}_p$, lexicographic smoothing results in an infeasible computational cost.

3.4 Line/plane relaxation methods

An alternative way to improve the smoothing properties of a multigrid method is to use block iterative methods (Arms et al. 1956) such as block Successive Overrelaxation (similar to Gauß-Seidel) (Evans and Biggins 1982) or the block Jacobi method (Ferguson 1986). In the context of anisotropic partial differential equations, line successive overrelaxation and plane successive overrelaxation are popular choices (Trottenberg et al. 2007). Equal to the case of coupled point SOR, the status update reads

$$\boldsymbol{u}_{i+1} = \boldsymbol{u}_i + \left(\boldsymbol{L}_{L/P} + \frac{1}{\omega}\boldsymbol{D}_{L/P}\right)^{-1} \cdot \left(\boldsymbol{f} - \boldsymbol{K}\boldsymbol{u}_i\right) \quad ,, \tag{9}$$

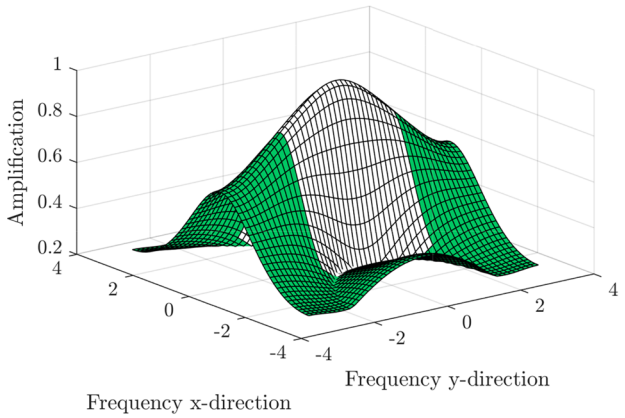

(a) Lines oriented into fiber direction.

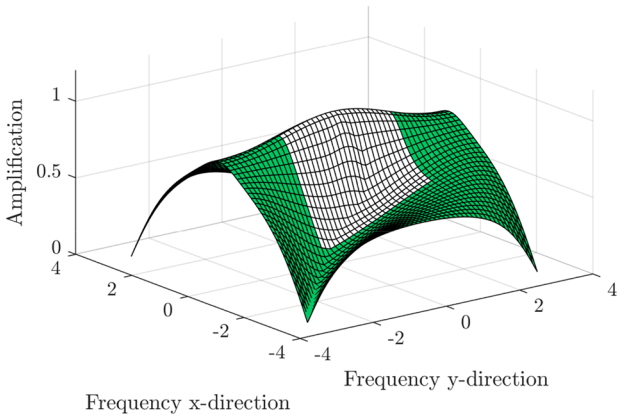

(b) Lines perpendicular to fiber direction.

Fig. 8 Amplification factors from the local Fourier analysis of line SOR smoothing with $\omega = 1$ for Balsa wood. The x- and y-axis represent the frequency of the error of the state in x-/y-direction. The z-axis represents the corresponding amplification factor. For visualization reasons, the frequency in z-direction is set to 0

where the matrix $\boldsymbol{D}_{L/P}$ is a block diagonal matrix that contains couplings between different degrees of freedom of the same box (line/plane). The lower triangular matrix $\boldsymbol{L}_{L/P}$ is chosen such that $\boldsymbol{K} = \boldsymbol{L}_{L/P} + \boldsymbol{D}_{L/P} + \boldsymbol{L}_{L/P}^T$. When choosing the lines that are oriented in the same direction as the stiffest material direction, substantial improvements in the smoothing are obtained. Application of the local Fourier analysis to x-line SOR for Balsa wood with $\eta = 0, \varphi = 0, \theta = 0$ shows completely different behavior to the decoupled SOR method. Figure 8a shows the amplification factors for different frequencies in the x- and y-directions. In difference to classic lexicographic SOR (as shown in Fig. 7), line SOR also shows good smoothing properties for high frequencies in the y-direction. In consequence, the overall smoothing factor is much better with $\mu_{loc} < 0.8$ instead of 0.9. If, however, the lines are not oriented into the stiffest material direction, no advantage is found compared to coupled successive over-relaxation (See Fig. 8b). Similar observations are done for plane SOR.

For both relaxation algorithms, again, the smoothing properties depend on the node numbering. When using the multicolor numbering, the colors contain lines/planes that do not have any connections to each other. In this case it is sufficient to approximate the solution of (9) using one V-cycle of the multigrid method for every plane/line (Thole and Trottenberg 1986) separately. Alternatively, the system of equations could be solved using conjugate gradients. Own investigations showed that a desired tolerance of less than 10^{-2} often does not give any improvements for the global multigrid solve.

3.5 Direct comparison of smoothing methods

Besides computing the amplification factor function for a single orientation, the local Fourier analysis is also able to compute the smoothing factors for several orientations. Figure 9 shows smoothing factor maps for different smoothing algorithms. There, the smoothing factors are depicted for all rotations φ and θ. The rotation η is set to zero for visualization reasons. Additionally, Table 1 presents the minimum, maximum and mean value as well as the orientations of best/worst performance for all considered methods.

For the Jacobi method, the damping factor $\omega = 0.3$ is chosen since it is an appropriate value for $\varphi = 0, \theta = 0$. However, instabilities occur for several orientations where both angles are rotated by approximately $\pm 15°$. Using $\omega = 0.25$ instead, unstable regions are removed at the cost of slightly worsened smoothing factors at the other orientations. The best values are found at orientations that align to the coordinate axes since these cases contain no couplings between degrees of freedom at the same node. There, the smoothing factor reaches values around 0.98.

Like the Jacobi method, the decoupled lexicographic SOR method shows orientation-dependent smoothing properties. Considering $\omega = 1$ (i.e., Gauß-Seidel method) the qualitative appearance of good and poor performance is similar to the Jacobi method. However, the absolute quantities are significantly better, with values between 0.84 and 0.96. The best performance is obtained for orientations that are near $\varphi = 0, \theta = 0$. This is explained by the node-numbering-dependent properties. In the current case, the nodes are numbered line-wise with the lines oriented in the x-direction. This means that a strong coupling in x-direction is implemented in the smoothing process. Hence, good

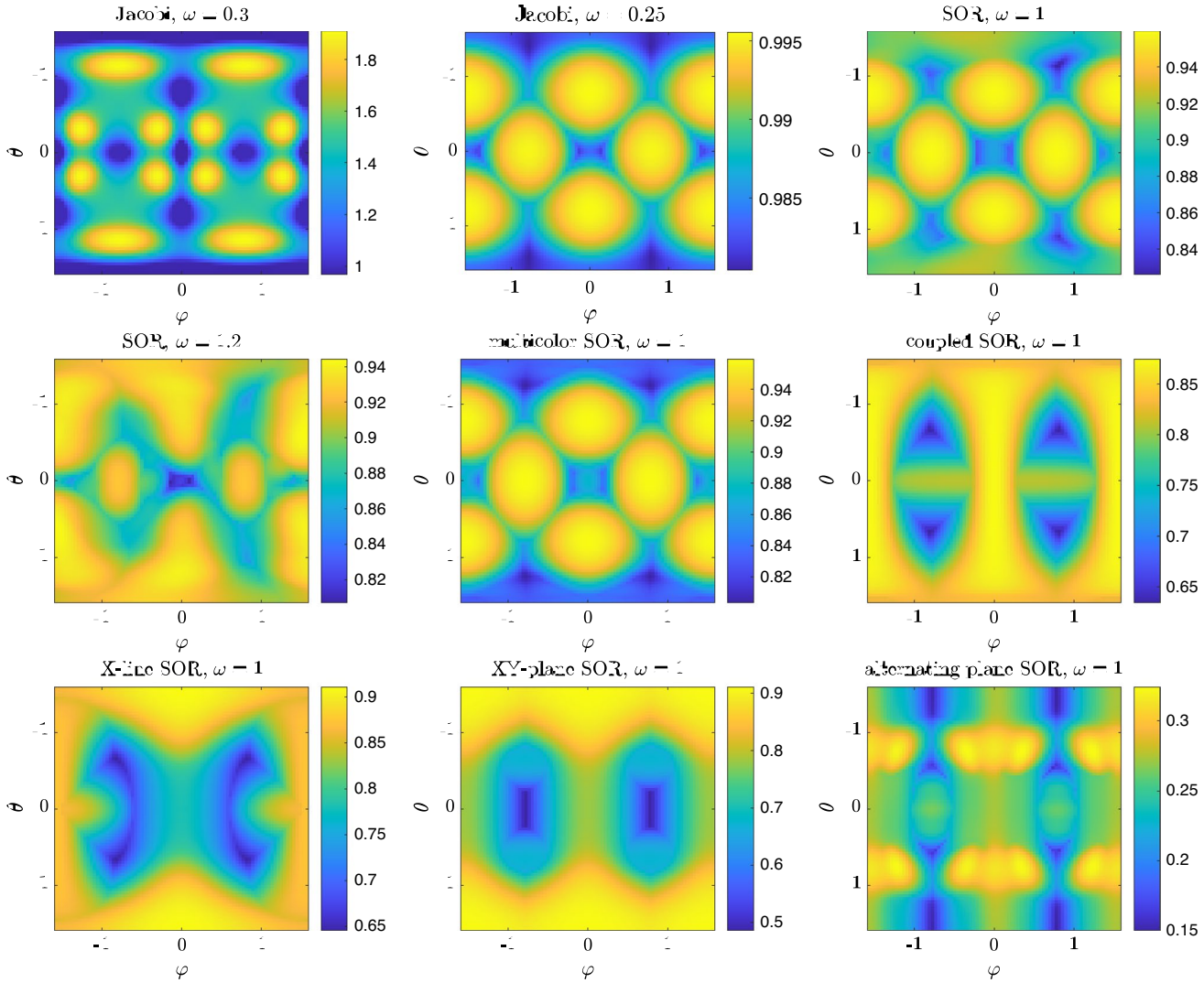

Fig. 9 Smoothing factors μ_{loc} for different smoothing algorithms considering Balsa in different orientations φ, θ computed using the local Fourier analysis. The first rotation around the x-axis is set to zero, i.e., $\eta = 0$. The colors indicate the smoothing factors values

Table 1 Smoothing factors and orientations with best or unstable behavior for different smoothing algorithms obtained using local Fourier analysis

Smoothing method	Smoothing factor			Best/unstable
	Minimum	Maximum	Mean	Orientation
Jacobi $\omega = 0.3$	0.976	1.18	1.01	Unstable at $\approx \pm 15°$
Jacobi $\omega = 0.25$	0.98	0.996	0.99	Coordinate axes
SOR $\omega = 1$	0.83	0.96	0.92	x-direction
SOR $\omega = 1.2$	0.81	0.94	0.91	x-direction
Multicolor SOR $\omega = 1$	0.80	0.96	0.90	Coordinate axes
Coupled SOR $\omega = 1$	0.63	0.87	0.81	$\approx \pm 45°$
X-line SOR $\omega = 1$	0.65	0.91	0.81	x-direction
XY-plane SOR $\omega = 1$	0.49	0.91	0.78	x-y-plane
Alternating plane SOR $\omega = 1$	0.15	0.32	0.26	All directions

smoothing properties are obtained for the stiffest direction pointing in x-direction. If the numbering was line-wise with

lines oriented into the y-direction, the best smoothing properties are obtained for $\varphi = 90°, \theta = 0$. Increasing the damping factor to $\omega = 1.2$, this effect is even amplified, leading to superior smoothing factors at $\varphi = 0, \theta = 0$ and inferior factors for large rotations. However, considering all orientations, the mean smoothing factor is improved by less than 1%. Higher damping factors do not improve the performance anymore, but lead to unstable methods.

In difference to the lexicographic ordering, the multicolor ordering does not have a directed numbering and hence, also does not show superior behavior for a certain coordinate axis direction. Besides this effect, the behavior is nearly equal to the lexicographic version.

Considering couplings at single nodes by utilization of the coupled multicolor SOR smoother with $\omega = 1$ improves the performance for orientations that are not aligned with the coordinate axes. Especially at orientations where both rotations are near $\pm 45°$, coupled multicolor SOR shows its best performance with smoothing factors around $\mu_{loc} = 0.65$. This comes from the fact that the coupling between the degrees of freedom of a single node reaches its maximum for rotations of approximately $\pm 45°$.

By using line or plane smoothing, superior smoothing factors are obtained for orientations that align with the line or plane. There, the smoothing factor is improved by more than 15% compared to coupled smoothing. Since line and plane smoothing also include all couplings at the same node, they also work well for all angles, where the coupled SOR method worked well. In consequence, the smoothing factor is less than 0.8 for many angles. However, as expected, the performance is rather bad for material orientations that are perpendicular to the smoothing line or plane (e.g., $\theta \approx \pm 90°$).

A more robust formulation is the alternating plane smoothing. There, plane smoothing is done for the x-y, y-z and x-z planes sequentially. This obviously comes at the cost of three smoothing swipes of single-plane smoothing. However, application of the local Fourier analysis reveals that alternating plane smoothing shows good performance for all orientations (including these, where the previous methods performed badly) with smoothing factors of less than $\mu_{loc} < 0.33$. In fact, it performs better than three applications of xy-plane smoothing for many material orientations.

Based on these results, the alternating plane smoothing is clearly the best smoothing approach. However, despite the smoothing factors, the previously mentioned algorithms have substantially different computation times and memory demands. The required number of scalar multiplications and a relative computation time for a naive Matlab implementation are shown in Table 2. The corresponding assumptions and detailed derivations are found in b. Paying attention to the computation times, the ranking depends on the specific orientations. Especially coupled successive overrelaxation and line successive overrelaxation seem to be very competitive since they are much less computationally costly than alternating plane smoothing. However, there are many effects in practical application that are not considered by the local Fourier analysis. Therefore, the smoothing algorithms are applied in the context of practical optimization problems.

4 Numeric analysis of existing smoothing methods

To validate the results of the local Fourier analysis and extend them to real topology optimization problems, different smoothing methods are analyzed regarding their properties when solving the finite element equation. In the following analysis, the required number of iterations is computed for four different designs. In the first experiment, the special case of constant coefficients (i.e., constant density field, constant orientations) is considered, which is as close as possible to the assumptions made for the local Fourier analysis. Afterwards, the more general cases of non-constant orientations and/or non-constant densities are considered. Again, Balsa wood is used as material. For the application of the multigrid solvers to different problems (4.2 to 4.5), the V-Cycle multigrid method is used as a preconditioner to the conjugate gradient method, since this is state of the art in the field of engineering optimization. Very tight solver tolerances of 10^{-10} are considered to get reproducible results, and only one smoothing swipe is applied on each grid. The

Table 2 Required number of multiplications per node for different smoothing algorithms for the case that the global stiffness $\boldsymbol{K}$ is available or not

	Smoothing method					
	Jacobi	SOR	Coupled SOR	Line SOR	Plane SOR	Alternating SOR
$\boldsymbol{K}$ available	~ 250	~ 360	300–500	~ 800	~ 2000	~ 5500
$\boldsymbol{K}$ not available	~ 580	~ 1200	700–850	~ 1100	~ 2500	~ 6000
Observed time Matlab	100%	200%	250%	450%	800%	2400%

The observed time using a naive (sequential) Matlab implementation is given relative to the Jacobi method, where $\boldsymbol{K}$ was available

damping factor is set to $\omega = 0.25$ for the Jacobi method, since the local Fourier analysis reveals that higher values lead to unstable behavior. For all other methods, the damping factor is set to $\omega = 1$, since this case corresponds to Gauß-Seidel methods. According to the local Fourier analysis, increasing the value does not cause significantly improved smoothing. The decoupled multicolor SOR method is not considered since it is always inferior to the coupled version at similar computational cost.

4.1 Example considered

For the analysis examples with non-constant densities, the density field is computed using a topology optimization of a cantilever beam, which is discussed in more detail in Sect. 7.1. The corresponding problem is taken from Peetz and Elbanna (2021).

The design space and the boundaries are depicted in Fig. 10a . The problem consists of a cuboid-shaped design space that is discretized using a structured mesh of $64 \times 32 \times 32$ isometric hexagonal finite elements. The low number of finite elements is chosen such that the direct solve can be applied already at the second grid in order to enable an analysis of the two grid method. The model is clamped on the back surface and loaded by a line load on the lower front edge. For the design generation, isotropic linear elastic material behavior with a Poissons's ratio of 0.3 is considered. The densities are filtered using the PDE filter (Lazarov and Sigmund 2011) with a filter radius of 2 times the element edge length and afterwards penalized using the modified SIMP approach (Sigmund 2007). Like in Peetz and Elbanna (2021), a continuation scheme is applied for the penalization parameter p. Starting from 1, p is increased by 0.25 every 20 iterations up to a maximum value of $p = 4$. At every change of p a new optimization is started using the previous design as the initial guess. Considering an allowed volume fraction of 12%, the optimization using the method of moving asymptotes (Svanberg 1987) leads to the final design shown in Fig. 10b . The result is qualitatively similar to the design gained in Peetz and Elbanna (2021). However, visible differences are caused by a different discretization, filter type

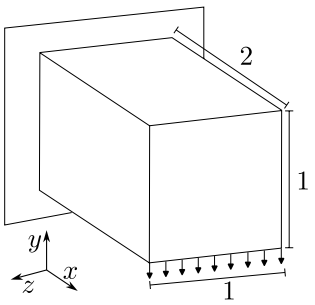

(a) Design space and boundary conditions for the topology optimization problem.

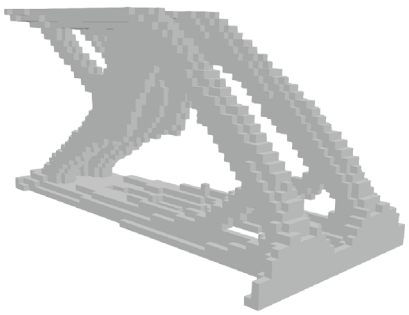

(b) Final design of the isotropic topology optimization.

Fig. 10 Compliance topology optimization example of an cantilever used for the following numeric experiments

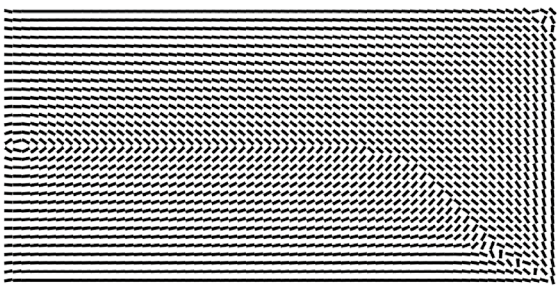

(a) Orientation field for the constant density field.

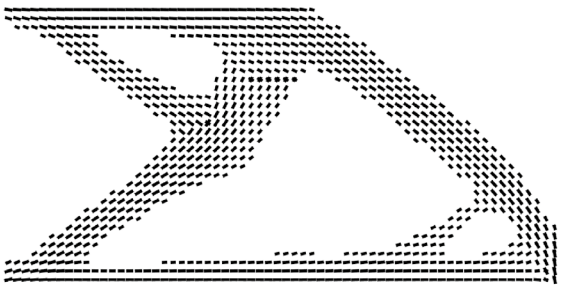

(b) Orientation field for the non-constant density field.

Fig. 11 Side view of the orientation fields for the example problems considering constant and non-constant densities. The orientations are aligned to the first principal stress direction

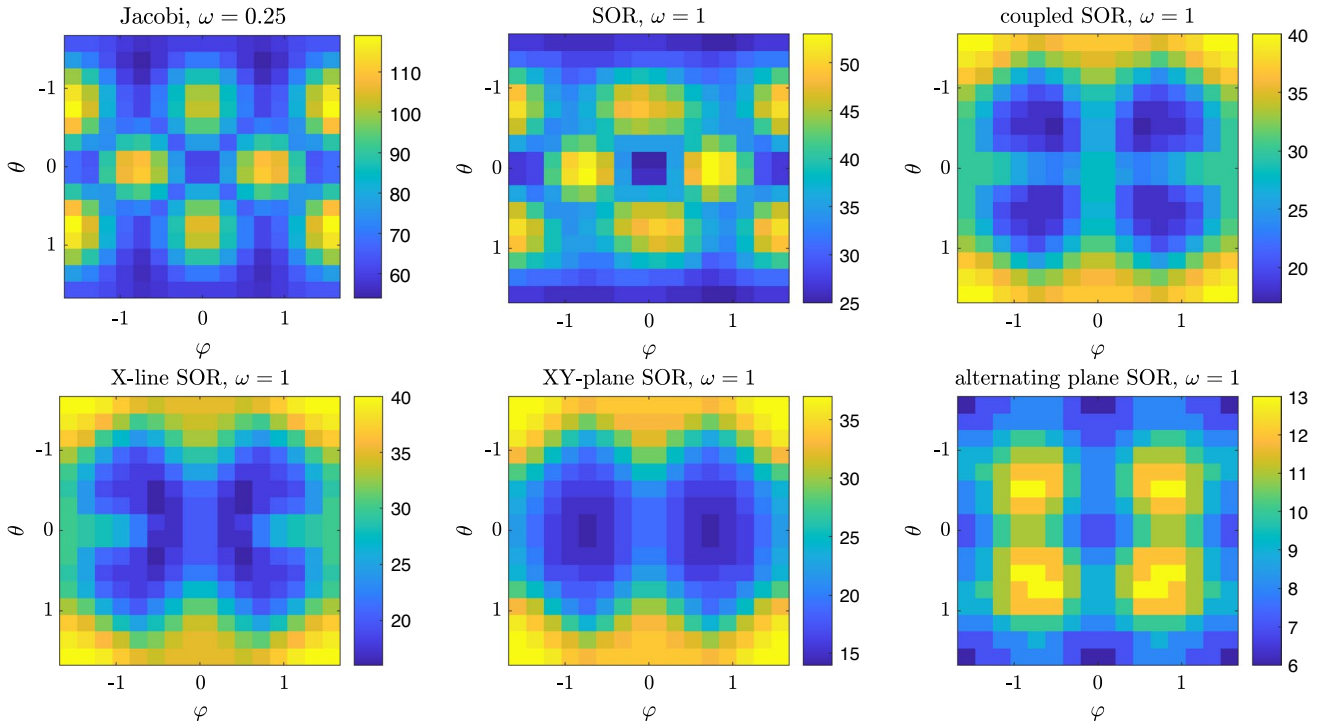

Fig. 12 Required number of iterations for the multigrid method to reach a relative tolerance of 10^{-10} for different constant material orientations φ, θ of Balsa wood. Here, the elasticity equations of the example problem 10a with constant densities is solved using 2 grids. The colors indicate the required number of iterations

and relative filter radius. Especially the very coarse discretization in combination with a low volume fraction leads to many elements with intermediate densities. As previously mentioned, numerical experiments are also done for spatially varying orientations combined with constant and optimized topology. For simplicity, the material is oriented into the principal stress directions. Thereby, the rotation around the x-axis is set to zero, i.e., $\eta = 0$. A 2D-cut of the orientation field is shown in Fig. 11.

4.2 Application of methods to example with constant densities and constant orientations

First, the multigrid solver is applied to the example problem 10a with constant densities and constant orientations. Figure 12 shows the number of iterations[1] needed when using 2 grids, such as assumed in the local Fourier analysis. Qualitatively, the results are equivalent to the local Fourier analysis. For orientations where low smoothing factors were obtained, the number of iterations is also low. Additionally, the ranking of smoothing methods is the same. However, the Jacobi method performs better than expected. For the orientation $\varphi = 0, \theta = 0$ the smoothing factor $\mu_{loc} = 0.98$ was obtained. To reduce the high-frequency error to 90%, which is the smoothing factor of lexicographic SOR, approximately 5 smoothing swipes are required ($0.98^5 \approx 0.9$). However, the experiments only show a difference of factor 2. The improved performance of the Jacobi method is explained by beneficial effects of the outer conjugate gradient solver. In additional numerical experiments, the authors used the multigrid method as a standalone solver. There, the iteration numbers were a factor of 2 to 5 higher for all smoothing methods, and especially the Jacobi method performed approximately 5 times worse than the lexicographic SOR method. In practical application, rather 3–5 grids are used than only 2 grids to reduce the cost of the coarse grid solve (Amir et al. 2014; Peetz and Elbanna 2021). Repeating the same experiment with four grids, the numbers of iterations are similar to the results shown in Fig. 12. The values are increased by up to two in only a very small number of orientations.

[1] Iterations here refer to the solution of the equation system, not to the number of optimization iterations.

Table 3 Number of iterations to compute the deformations of example problem 10a, where the orientations of the Balsa wood are set to the principal stress direction or are spatially random

Example	Multigrid approach	Smoothing method					
		Jacobi	SOR	Coupled SOR	Line SOR	Plane SOR	Alternating SOR
Stress-aligned orientations	2 grids	92	41	29	28	27	8
	4 grids	94	43	31	29	28	9
Random orientations	4 grids	59	32	30	29	28	14

The V-Cycle procedure is used with the desired tolerance 10^{-10}

4.3 Application of methods to example with constant densities and optimized orientations

Considering the orientation field presented in Fig. 11a in combination with constant densities, the iteration numbers represented in Table 3 are obtained. There, the two grid cycle as well as the four-grid cycle are applied. The achieved numbers of iterations are approximately the mean of the iterations required for all included orientations. Hence, the non-constant orientations do not cause extra problems for the multigrid solver. In fact, there is an opposite effect. Possible bad orientations in the design are balanced by good orientations leading to an intermediate performance. The same effect is observed in the case of uncorrelated random orientations. There, the balancing effect is even more present. Also, using multiple grids does not worsen the convergence speed.

4.4 Application of methods to example with optimized topology and constant orientations

Application of the multigrid method to the topology optimized design shown in Fig. 10b with constant material orientations and two grids leads to the iteration numbers shown in Fig. 13. The general relationship of iteration number and orientation is similar to the case of constant densities, but the absolute numbers increase. While the iteration numbers are only increased by 10%-20% for Jacobi and lexicographic SOR, the numbers are approximately doubled for the multicolor methods, still showing better performance. This is caused by two reasons. First, the problem of anisotropy seems to be rather independent of the problem of high contrasts. Hence, the number of iterations is increased by approximately the same amount for all methods, which leads to a higher relative increase for the methods that performed better for constant densities. Second, the multicolor pattern strictly requires the low-frequency errors to be suppressed by the coarse grid solve. For more details, see the derivation of the local Fourier analysis in Trottenberg et al. (2007). In the context of high contrast designs, this requirement is not fulfilled anymore, since structural details of the fine grid are not properly represented on the coarse grid.

In difference to the case of constant densities, the multicolor smoothers also suffer from an inaccurate solve of the state update Eq. 9. Using only one swipe of the corresponding 1D/2D multigrid method even leads to divergence of the overall solver. This is caused by poor performance of the multigrid method in the case of high-contrast designs on more than two grids (Peetz and Elbanna 2021). However, solving the line/plane problem with an accuracy of at least 10^{-2} leads to less than 10% additional iterations for the overall solve.

When using the multigrid method with four grids instead of two grids, the numbers of iterations totally explode for some orientations. Instead of 30–130 iterations, 300–450 iterations are required. The corresponding figure is found in c. However, numerical experiments show that a similar loss of performance is also found for isotropic materials, such as steel, where the number of iterations grows by a factor of 5. Hence, it is expected that the reasons are equal to the case of isotropic topology optimization (e.g., discussed in Amir et al. (2014); Peetz and Elbanna (2021)). There, the major problem is that the details of the fine grid are not properly represented on the coarse grid.

A simple fix to improve the convergence of the multigrid method with many grids and topology optimized designs is to use several smoothing steps on the coarse grids or to apply a different multigrid cycle. Since the convergence is good when using only two grids, the problems must be caused by the coarse grids. In consequence, improving the components at coarse grids also improves the overall performance.

When using the W-Cycle instead of the V-Cycle, the computational cost is increased by approximately 15% per iteration. Application of the W-Cycle to the example with optimized topology with four grids leads to the iteration numbers presented in Fig. 14. Compared to the V-Cycle, the number of iterations drops by 30% to 50%, which is still significantly more than in the case with 2 grids. Additionally,

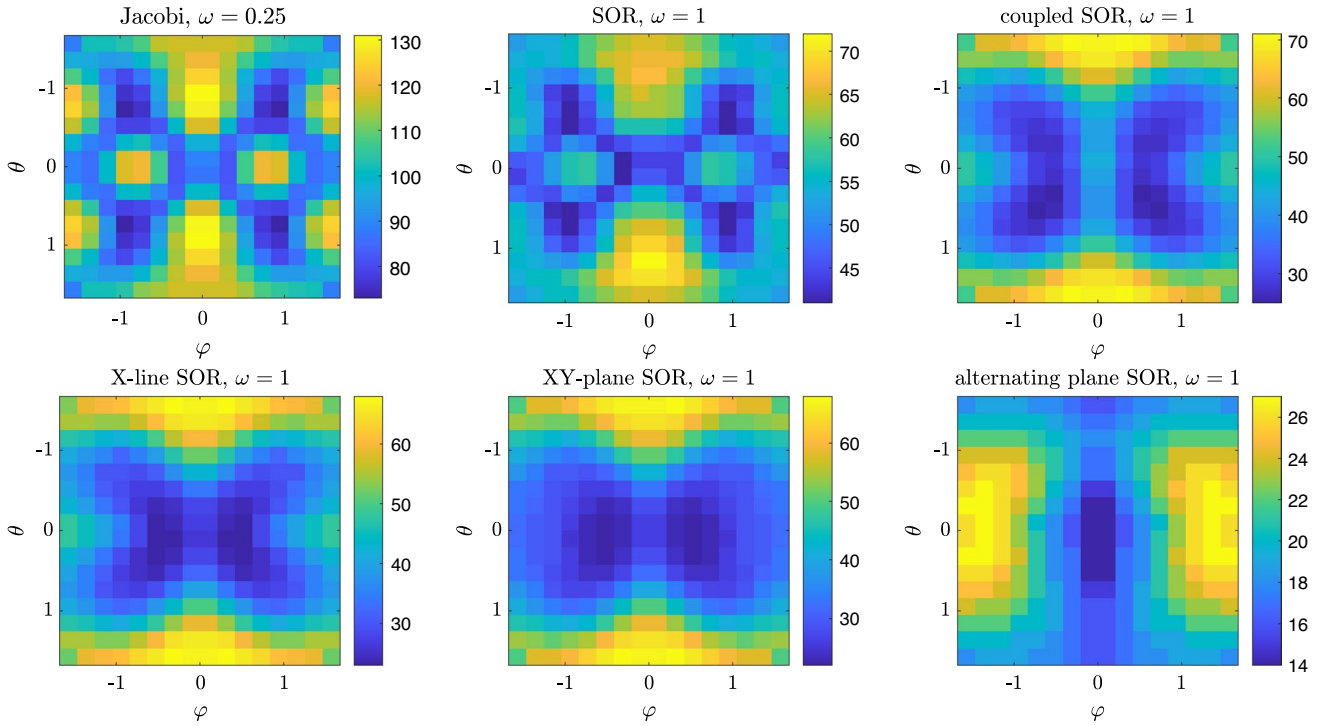

Fig. 13 Required number of iterations for the multigrid method to reach a relative tolerance of 10^{-10} for different constant material orientations φ, θ of Balsa wood. Here, the elasticity equations of the example problem 10b with optimized densities is solved using 2 grids. The colors indicate the required number of iterations

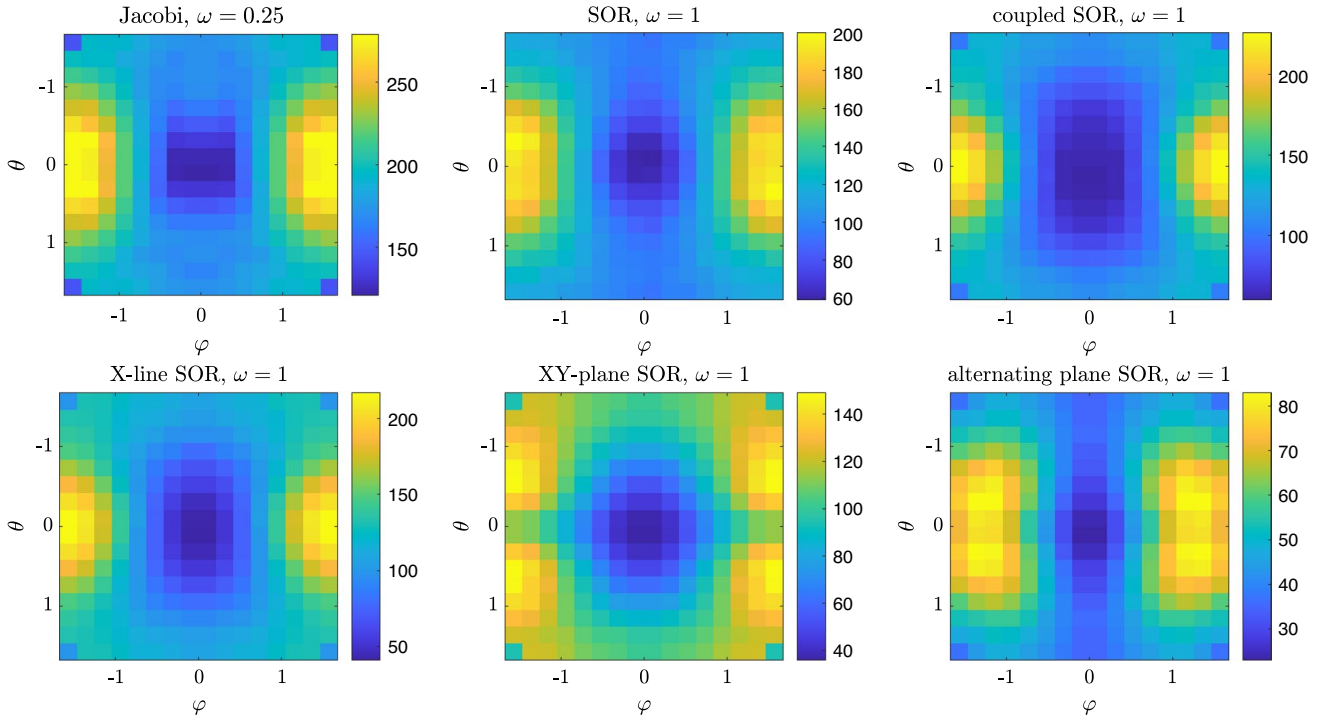

Fig. 14 Required number of iterations for the multigrid method to reach a relative tolerance of 10^{-10} for different constant material orientations φ, θ of Balsa wood. Here, the elasticity equations of the example problem 10b with optimized densities is solved using the W-Cycle with 4 grids. The colors indicate the required number of iterations

the general shape of the iteration number plot is fundamentally changed compared to the case with 2 grids. Especially orientations with $\varphi = 0, \theta = 0$ now show best performance, which might be explained by the fact that the shape of the topology is also oriented to the x-axis.

4.5 Application of methods to example with optimized topology and varying orientations

Combining non-constant densities with stress-aligned orientations shown in Fig. 11b leads to the iteration numbers presented in Table 4. There, all previously discussed cases, i.e., two grids, four grids and four grids with W-cycle, are considered. For comparison, also the number of iterations for spatially random orientations and isotropic steel as material are shown.

In the case of two grids, the number of iterations is similar to the case with constant densities. Considering optimized orientations, the number of iterations does not explode when going to four grids. In fact, the values only increase by less than 25%. Again, good orientations balance bad orientations, leading to overall good performance. Unexpectedly, this means that the required number of iterations is even lower than when considering isotropic steel as material. The reason is found in the specific orientation field. Since the material is oriented into the principal stress direction, the principal material direction aligns with the structural elements. The stiffness in fiber direction is much higher than the orthogonal stiffness and the shear stiffness. In consequence, small errors in deformations at the transition zones have less influence on the force residual. This effect does not occur in the context of completely random orientations. There, only the balancing effect between good and bad orientations is observed, leading to worse values than for the isotropic material. When using the W-cycle instead of the V-cycle for multiple grids, again, the number of iterations drops significantly.

Table 4 Number of iterations to compute the deformations of the topology optimized example problem 10b, where the orientations of the Balsa wood are set to the principal stress direction or are spatially random

Example	Multigrid approach	Smoothing method					
		Jacobi	SOR	Coupled SOR	Line SOR	Plane SOR	Alternating SOR
orientation stress-aligned	2 grids	100	48	29	28	28	11
	4 grids	104	56	36	34	34	21
	W-Cycle 4 grids	102	50	31	29	28	15
random orientations	4 grids	266	185	184	185	161	99
isotropic	4 grids	130	97	77	77	70	49

The desired solver tolerance is set to 10^{-10}

Fig. 15 Algorithm for computing optimal damping factors in the context of spatial Jacobi smoothing. This preprocessing must be done only once for every material

```
Generate vectors of angles η = [−π/2 ... π/2]^T, φ = [−π/2 ... π/2]^T, θ = [−π/2 ... π/2]^T
Generate vector of damping factors ω = [0 ... 1]^T
Initialize lookup table ω_opt
for i_η
  for i_φ
    for i_θ
    Initialize smoothing factor vector μ_loc
      for i_ω
        Compute smoothing factor μ_loc,i_ω = μ_loc(η_i_η, φ_i_φ, θ_i_θ, ω_i_ω) using LFA
      end
      Find index i_opt of lowest value of μ_loc
      ω_opt,η_i_η,φ_i_φ,θ_i_θ,ω_i_ω = ω_i_opt
    end
  end
end
Compute intermediate values of ω_opt using a response surface
```

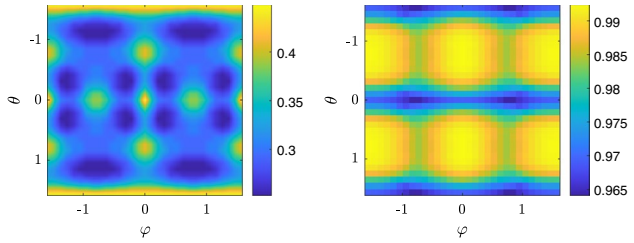

Fig. 16 Optimal damping factor ω (left) and resulting smoothing factors μ_{loc} (right) for Jacobi smoothing with Balsa for different orientations. The values are obtained using local Fourier analysis. The colors indicate the optimal damping factors (left) and the resulting smoothing factors (right). The angle η is set to zero for visualization reasons

5 New approach: spatial smoothing

The previous analyses showed that the (decoupled point) Jacobi method does not perform as well as coupled or box smoothers. However, especially in the context of topology optimized designs, the difference is not substantial (factor 2–4). On the other hand, the Jacobi method is simple, easy to implement, and very fast in the evaluation. The most crucial component is to choose the damping factor ω properly. In difference to the SOR schemes, where $\omega = 1$ is stable for all situations, the Jacobi method is stable for different damping factors for different materials and orientations. In Luo et al. (2024) it is proposed to compute optimal damping factors using an eigenvalue analysis of the true iteration matrix. This leads to good performance of the solution process, but it requires the expensive solution of an eigenvalue problem.

In the current publication, we propose a similar approach. However, the focus lies on different materials with spatially varying orientations. Hence it is proposed to use different damping factors for every node instead of one global value. Therefore, "optimal" damping factors are computed for all possible material orientations using the local Fourier analysis and stored in a lookup table. These values are only computed once for every material and do not change. During the (material orientation and) topology optimization, the optimal damping factors are extracted from the lookup table for every element separately. Afterwards, the nodal damping factors are computed from the elemental values by taking the volume-weighted average of all surrounding elements. Finally, the spatial damping factors are applied to the Jacobi method by

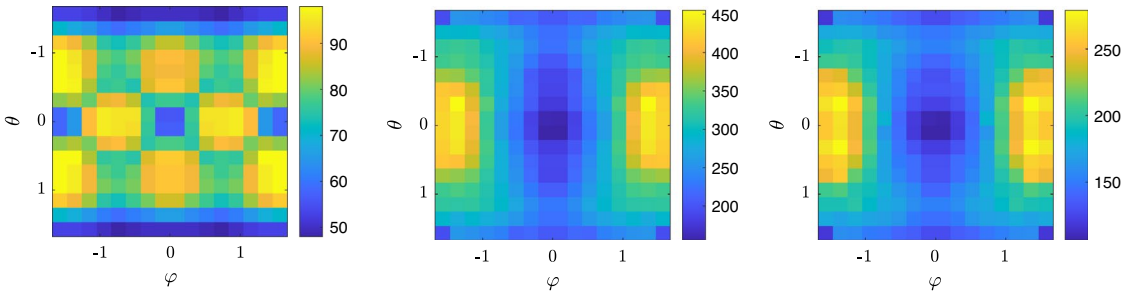

(a) Initial design, V-Cycle. (b) Optimized design, V-Cycle. (c) Optimized design, W-Cycle.

Fig. 17 Required number of iterations for the multigrid method using spatial Jacobi smoothing to reach a relative tolerance of 10^{-10} for different constant material orientations φ, θ of Balsa wood. Here, the elasticity equations of the example problems 10b and a are solved using 4 grids. The colors indicate the required number of iterations

Table 5 Number of iterations to compute the deformations of example problem 10a, where the orientations of the Balsa wood are set to the principal stress direction

Orientation field	Density field	Cycle type	Smoothing method		
			Spatial Jacobi	Jacobi with $\omega = 0.25$	Improvement (%)
Stress-aligned orientations	Initial design	V	76	94	20
	Optimized design	V	86	104	17
	Optimized design	W	82	102	20
Random orientations	Optimized design	V	248	266	7
	Optimized design	W	147	163	10

Four grids and a relative tolerance of 10^{-10} are applied

$$\boldsymbol{u}_{i+1} = \boldsymbol{u}_i + \boldsymbol{\omega D}^{-1} \cdot \left(\boldsymbol{f} - \boldsymbol{K u}_i\right) \tag{10}$$

with

$$\boldsymbol{\omega} = \begin{pmatrix} \omega_1 & 0 & 0 & \dots \\ 0 & \omega_2 & 0 & \dots \\ 0 & 0 & \omega_3 & \dots \\ \vdots & \vdots & \vdots & \ddots \end{pmatrix} . \tag{11}$$

A pseudo-code for computing the optimal factors is shown in Fig. 15. First, linearly spaced realizations of angles $\eta, \varphi, \theta \in [-\frac{\pi}{2}, \frac{\pi}{1}]$ and damping factors $\omega \in [0, 1]$ are generated. Afterwards, the local Fourier analysis is applied to every combination of angles and damping factors. The damping factors leading to the best local smoothing factor for each combination of angles is stored as the corresponding optimal damping factor. After the whole procedure, intermediate values may be interpolated using a fitted response surface.

For the example of Balsa wood, the "optimal" damping factors and the corresponding smoothing factors resulting from a local Fourier analysis are shown in Fig. 16. Here, the angles η, φ, θ are spaced by $\frac{\pi}{30}$ and the damping factor ω is spaced by 0.01. Application of spatial Jacobi smoothing to the example problem 10a with constant orientations leads to the iteration number plots shown in Fig. 17. There, both designs (initial and topology optimized) are used in combination with four grids. Since the orientations are constant, the damping factor ω is also constant. However, it is adjusted to the occurring orientation instead of using the standard value $\omega = 0.25$. The spatial Jacobi method is stable for all orientations. Compared to a damping factor of $\omega = 0.25$, the number of iterations is reduced by up to 20%, depending on the specific orientation.

A similar improvement is obtained when considering orientations that are aligned with the principal stress direction. Table 5 shows the iteration numbers for both designs and both cycles for four grids. Here, actually spatial damping factors are practically used with values $\omega = 0.25...0.45$. In all situations, the number of iterations is reduced by more than 15%. Considering spatially random orientations instead, the improvement is still 7–10%.

Using spatial Jacobi smoothing instead of classic Jacobi smoothing, the computation time per iteration increases less than 1%. Additionally, the lookup table must be computed once. Using a workstation, this takes approximately 10 min, independent of the size of the topology optimization problem.

6 Recommendations to choose smoother for different situations

Combining the analysis of the computational effort with the obtained numbers of iterations shows that plane smoothing and alternating plane smoothing usually do not improve the overall computation time. The reduction in solver iteration is fully covered by a significant increase in cost for a single smoothing swipe.

The newly presented spatial Jacobi smoothing always outperforms standard Jacobi smoothing since it reduces the iterations without increasing the cost. Hence, it should always be preferred.

For the remaining methods, the situation is less obvious. Lexicographic SOR reduces the number of iterations by approximately 50–70% compared to spatial Jacobi, but it increases the cost per smoothing swipe. Still, it might outperform Jacobi and spatial Jacobi by 10–20% considering the number of floating-point multiplications. However, there is a huge amount of indexing leading to higher observed computation times in Matlab. Additionally, it is not parallelizable. In the authors opinion, the possible advantages are too low to switch to lexicographic SOR.

If the material orientation varies over the design domain, coupled SOR and line SOR reduce the required number of iterations by up to 70% to similar iteration numbers. Additionally, both methods parallelize well. Since coupled SOR requires significantly fewer operations than line SOR, it should be preferred in these situations. Depending on the efficiency of the implementation, it might outperform the spatial Jacobi method, and hence, could be preferred.

If the orientation field is (nearly) constant, the performance depends on the specific orientation as well as the density field. In many cases, the density field reduces the performance differences such that spatial Jacobi smoothing shows the best performance. However, especially at orientations that do not align with the grid, coupled SOR outperforms all competitors. On the other hand, line SOR often outperforms all other methods if the lines align with the material orientation. For a good decision, the reader is advised to check the results of the local Fourier analysis.

7 Numeric optimizations

To validate the previous observations, several methods are used in a (material orientation and) topology optimization. The required number of multigrid iterations to reach a relative tolerance of 10^{-10} is tracked during the optimization process. For the topology optimization, the modified SIMP approach (Sigmund 2007) in combination with the PDE filter with consistent boundary conditions (Wallin et al. 2020) is used. To keep the examples as simple as possible, no continuation

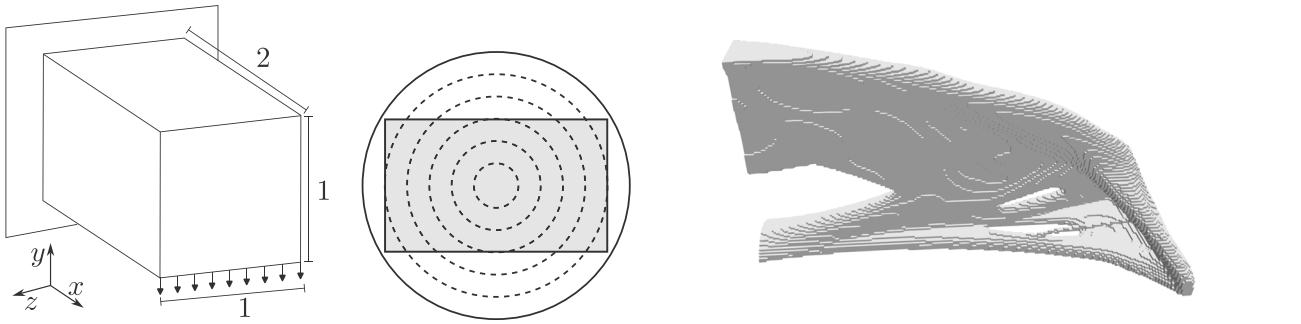

(a) Design space, loads and boundary conditions for the cantilever topology optimization.

(b) Position of the design space in the Balsa tree it is cut off.

(c) Optimized design of the cantilever example. Shown is the iso-cut where all elements with a density that is higher than 0.5 are shown.

Fig. 18 Optimization problem and result of the cantilever beam example

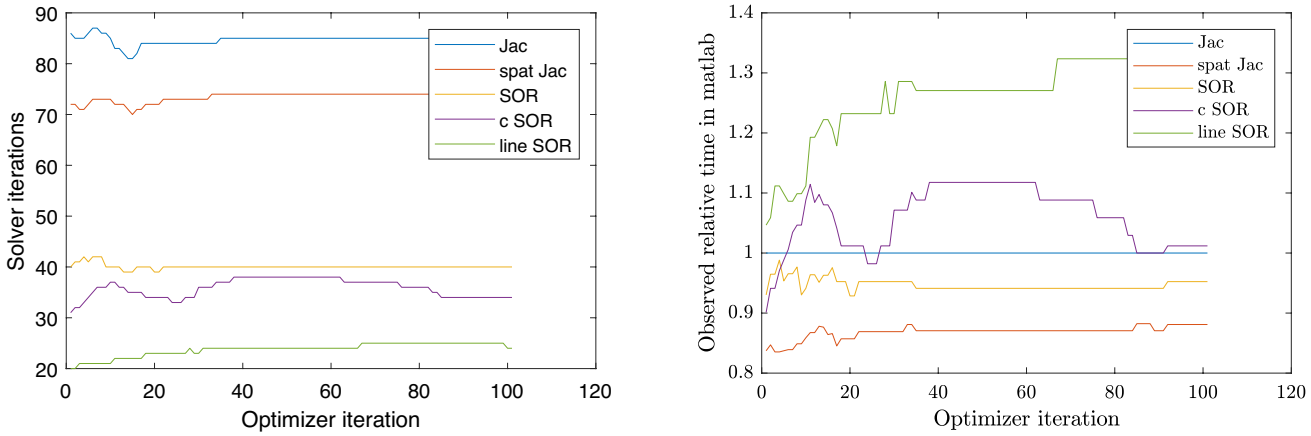

Fig. 19 Number of solver iterations (left) and observed computation time (right) during the optimization of the Balsa cantilever example for the following smoothing algorithms: Jacobi method ("Jac", $\omega = 0.25$, Sect. 3.1), spatial Jacobi method ("spat Jac", Sect. 5), lexicographic SOR ("SOR", Sect. 3.2), coupled multicolor SOR ("c SOR", Sect. 3.3) and line SOR (Sect. 3.4). The observed time is given relative to the Jacobi method

schemes are used. The optimizations are carried out using the method of moving asymptotes (Svanberg 1987) with the standard parameters. Only the initial move limit is set to 0.25 instead of 0.5. The optimizations are stopped after 100 iterations. In all cases considered, the relative change of the objective function is less than 10^{-4}.

7.1 Topology optimization of a Balsa wood cantilever beam

The first example consists of a simple compliance topology optimization of a cantilever beam. It is similar to the cantilever example in Aage et al. (2015). The optimization problem reads

$$\begin{aligned} \min_{\boldsymbol{\rho}} & f(\boldsymbol{\rho}) = \boldsymbol{u}^T \boldsymbol{K} \boldsymbol{u} \\ \text{s.t.}: \quad & V(\boldsymbol{\rho}) \leq 0.12 V_0 \\ & 0 \leq \boldsymbol{\rho} \leq 1 \\ \text{with}: \quad & \boldsymbol{K}(\boldsymbol{\rho}) \boldsymbol{u} = \boldsymbol{f} \end{aligned} , \tag{12}$$

where $\boldsymbol{\rho}$ represents the vector of pseudo densities, $V(\boldsymbol{\rho})$ the volume at the current design and V_0 the design space volume. The design space, loads and boundaries are depicted in Fig. 18a . It is discretized using $192 \times 96 \times 96$ finite elements. The filter radius is set to 0.03, and the minimal Young's modulus is set to $E_{min} = 10^{-9} E_0$. The volume fraction is set to 12%. As material, Balsa wood with the material properties listed in Appendix D.2 is used. The spatially different material orientations are chosen such that the axial

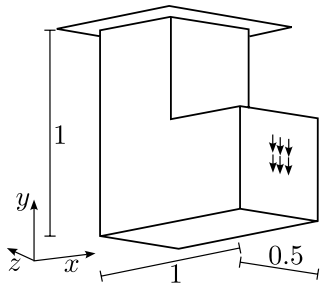

(a) Design space, loads and boundary conditions for the material orientation and topology optimization of the L-Beam example.

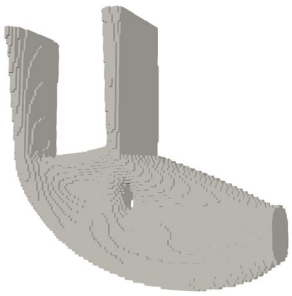

(b) Iso-cut at 0.5 of the density field of the optimized design of the L-beam example.

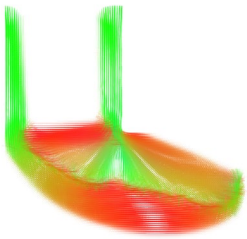

(c) Orientation field of the optimized design of the L-beam example. The colors highlight the orientations: green - aligned with y-axis, red - aligned with x-axis.

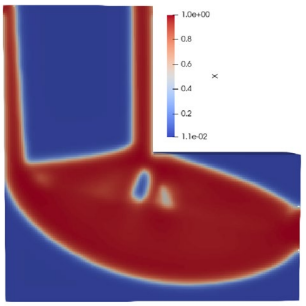

(d) Cut of the density field of the optimized design of the L-beam example. The cut is done at the model center.

Fig. 20 Optimization problem and result of the L-beam example

material axis points in the x-direction. To model imperfect growth and effects of branches, the axial axis is perturbed by random effects. The deviation in the axis is realized by perturbing the angles φ, θ using a Gaussian square exponential random field with the correlation length $l_c = 0.1$ and the variance $\sigma^2 = (18°)^2$. The radial and tangential axes are chosen to point in radial and tangential directions corresponding to the center of the design space, as depicted in Fig. 18b.

Overall, one optimization is done for each of the following smoothers using the W-Cycle multigrid preconditioned gradient solver with four grids: Jacobi method ($\omega = 0.25$), spatial Jacobi method, decoupled successive overrelaxation ($\omega = 1$), coupled successive overrelaxation ($\omega = 1$) and x-line successive overrelaxation ($\omega = 1$). The subproblems of the box smoother are solved using Jacobi preconditioned conjugate gradients with a tolerance of 10^{-3}. All optimizations converge to the exactly same design, which is depicted in Fig. 18c . Also, all numerical values are exactly the same.

The design is totally different from the result with isotropic material shown in Aage et al. (2015). The optimizer tries to exploit the anisotropic material behavior by reducing the average angle to the axial material direction. Due to the (asymmetric) random orientations, an asymmetric design is found.

Figure 19 shows the required number of solver iterations for every optimization step and all considered multigrid smoothers. Additionally, the figure shows the computation time relative to the Jacobi method in a naive sequential implementation (see Table 2). These results are consistent with previous findings. Spatial Jacobi reduces the required iteration number by 10–20% compared to Jacobi with $\omega = 0.25$. As expected, x-line successive overrelaxation shows the lowest number of iterations, while the point SOR methods are in between. Considering computation time, the spatial Jacobi method shows the best performance, whereas the line smoothing suffers from its high complexity. The absolute number of solver iterations stays relatively low because the W-Cycle is used and the topology aligns with the material orientation. This effect has already been observed in the previous analysis with orientations into principal stress direction.

7.2 Material orientation and topology optimization of a carbon fiber L-beam

The second example consists of a material orientation and topology optimization of a L-shaped beam. The design space is made of carbon fiber reinforced polymer with the material properties shown in D.1. The optimization problem reads

$$\begin{aligned} \min_{\boldsymbol{\rho},\boldsymbol{\Phi}} & f(\boldsymbol{\rho},\boldsymbol{\Phi}) = \boldsymbol{u}^T\boldsymbol{K}\boldsymbol{u} \\ \text{s.t.}: \quad & V(\boldsymbol{\rho}) \le 0.15 V_0 \\ & 0 \le \boldsymbol{\rho} \le 1 \\ & -2\pi \le \boldsymbol{\Phi} \le 2\pi \\ \text{with}: \quad & \boldsymbol{K}(\boldsymbol{\rho},\boldsymbol{\Phi})\boldsymbol{u} = \boldsymbol{f} \end{aligned} \quad , \tag{13}$$

where $\boldsymbol{\rho}$ represents the vector of pseudo densities, $\boldsymbol{\Phi}$ the material angles η, φ, θ, $V(\boldsymbol{\rho})$ the volume at the current design, and V_0 the design space volume. The density field

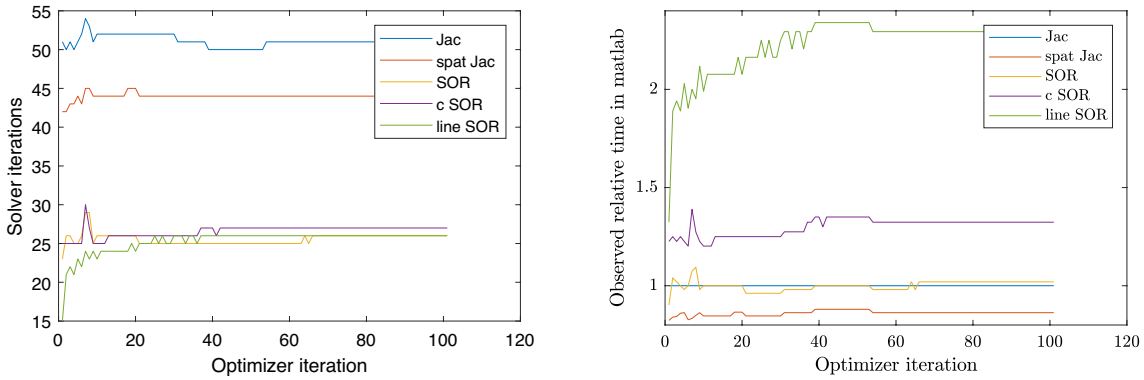

Fig. 21 Number of solver iterations (left) and observed computation time (right) during the optimization of the L-beam example for the following smoothing algorithms: Jacobi method ($\omega = 0.25$, Sect. 3.1), spatial Jacobi method (Sect. 5), lexicographic SOR (Sect. 3.2), coupled multicolor SOR (Sect. 3.3) and line SOR (Sect. 3.4). The observed time is given relative to the Jacobi method

is filtered using the PDE filter with consistent boundaries conditions and a filter radius of 0.03. The orientation field is filtered by a vector filter as described in Schmidt et al. (2020). There, the rotation angles are transformed to a direction vector. Afterwards, the direction vectors are filtered component-wise like the classic density filter in topology optimization. Again, the filter radius is set to 0.03. The problem is discretized using approximately 1,500,000 elements, and the volume fraction is set to 15%. As initial guess, all angles are set to 0°.

One full optimization is done for each of the following smoothers using the W-Cycle multigrid preconditioned gradient solver with four grids: Jacobi method ($\omega = 0.3$), spatial Jacobi method, decoupled successive overrelaxation ($\omega = 1$), coupled successive overrelaxation ($\omega = 1$) and x-line successive overrelaxation ($\omega = 1$). All optimizations lead to similar designs that are optically not distinguishable but have slightly different performance. Hence, the material orientation and topology optimization problem reacts very sensitive to small errors in the system solve. A iso-cut of the topology of the optimized design is shown in Fig. 20b , the orientation field in Fig. 20c. The general shape is similar to the results in literature, and the fibers are consequently aligned to the structural elements.

As in the cantilever example, the different smoothers lead to varying solution times. Figure 21 shows the required number of iterations to reach the desired tolerance of 10^{-10} for all optimization iterations. Additionally, the figure shows the computation time relative to the Jacobi method in a naive sequential implementation (see Table 2). As before, the standard Jacobi method shows the highest number of iterations. Using spatial Jacobi smoothing instead, the number of iterations drops by approximately 10–20% and leads to the lowest computation time. In contrast to the previous example, lexicographic SOR, coupled SOR and line SOR show similar iteration numbers. This is caused by the strongly varying material orientations and has also been observed in the previous analyses for Balsa. As shown in Fig. 20d , the final design shows clear contrasts and only contains intermediate densities at transition zones of the design surface. Hence, it is expected that the number of iterations grows as the design settles. In fact, the required number of iterations slightly increases during the first iterations. However, the final orientations are aligned with the structural elements, leading to the positive effects mentioned in Sect. 4.5.

8 Conclusions

In the current publication, the problem of simple Jacobi-smoothed multigrid methods with orthotropic materials is explained. Exemplary, Balsa wood and carbon fiber-reinforced polymers are considered. Different standard smoothers (namely the Jacobi method, lexicographic successive overrelaxation, multicolor coupled successive overrelaxation, multicolor line successive overrelaxation, multicolor plane successive overrelaxation and alternating multicolor plane successive overrelaxation) are analyzed using the local Fourier analysis and numeric experiments at different designs. There, constant material orientations as well as spatially varying orientations are considered. This way, the damping factor ω is chosen for the Jacobi method to be stable, and a new smoothing approach called spatial Jacobi smoothing is proposed. The new approach reduces the required number of solver iterations by up to 20% without increasing the cost per smoothing swipe.

When considering designs that have a developed topology, the problems of the multigrid method with orthotropic materials add up with the problems of contrast-rich designs. Depending on the material orientation field, the number of iterations totally explodes. In this case, using the

W-Cycle instead of the V-Cycle significantly improves the performance.

Based on the analyses, recommendations are given for choosing the smoothing algorithm for the multigrid method. For most more advanced smoothing algorithms, especially plane relaxation, the improved convergence properties do not balance the increased cost per smoothing swipe. Hence, the new approach is a good choice for many situations. However, depending on the implementation quality, multicolor coupled SOR and multicolor line SOR, might outperform the spatial Jacobi method.

Finally, the recommendations and results are validated at two different topology optimization examples.

Future research might address the generalization of the presented analyses and recommendations to the case of multi-material optimization, where also the type of material elastic symmetry varies element-wise.

Parallelization of multicolor SOR methods

All multicolor SOR methods use a chessboard-like node numbering (see Fig. 6b (b)), such that nodes of the same color have no couplings. On a structured 3D mesh, 8 colors are required. In the context of line smoothing, whole lines belong to the same color, such that the total number of numbers decreases to 4. Analogue, plane smoothing leads to 2 colors. In general, the state $\boldsymbol{u}_i$ can be rewritten as

$$\boldsymbol{u}_i = \begin{pmatrix} \boldsymbol{u}_{i,1} \\ \boldsymbol{u}_{i,2} \\ \vdots \\ \boldsymbol{u}_{i,n_c} \end{pmatrix}, \tag{A1}$$

where the partial vectors $\boldsymbol{u}_{i,c}$ correspond to the nodes of color c and n_c is the number of colors. Considering the coloring scheme, (7) is reformulated sequentially as

$$\boldsymbol{u}_{i+1,c} = \boldsymbol{u}_{i,c} + \left(\boldsymbol{L}_c + \frac{1}{\omega}\boldsymbol{D}_c\right)^{-1} \cdot \left(\boldsymbol{f}_c - \boldsymbol{K}_{c,:} \begin{pmatrix} \boldsymbol{u}_{i+1,1\ldots c-1} \\ \boldsymbol{u}_{i,c\ldots n_c} \end{pmatrix}\right), \tag{A2}$$

where $\boldsymbol{K}_{c,:}$ are the rows of the stiffness matrix $\boldsymbol{K}$ corresponding to color c, $\boldsymbol{u}_{i,1\ldots c-1}$ is the state vector corresponding to all previous colors and $\boldsymbol{u}_{i,c\ldots n_c}$ is the state vector of the current color and all following colors at iteration step i. The matrices $\boldsymbol{L}_c$ and $\boldsymbol{D}_c$ represent the lower diagonal and the diagonal part of the stiffness matrix entries corresponding to of color c. Due to the chosen coloring scheme, the matrix $\boldsymbol{L}_c$ only contains couplings between degrees of freedoms at the same node and hence, all nodes of the same color can be smoothed in parallel, whereas the different colors must be processed sequentially. In the case of coupled smoothing/line smoothing/plane smoothing, the matrix $\boldsymbol{L}_c$ vanishes and the matrix $\boldsymbol{D}_c$ becomes block diagonal. For more details, the reader is referred to Trottenberg et al. (2007).

Detailed analysis of computation time for different smoothing algorithms

The required computational cost of the different smoothing algorithms from Sect. 3.5 is determined based on the following assumptions and simplifications:

- Isometric 3D grid with first-order finite elements, standard grid transfer
- Cost of coarse grid solve is neglectable. This is true when using a sufficient number of grids. For example, five grids with approximately four billion elements on finest grid lead to approximately one million elements on the coarse grid. Then, a vector matrix product on the fine grid is more expensive than a (approximate) solve on the coarse grid.
- Perfect implementation such that computation time only depends on the number of multiplications
- The element stiffness matrices are already computed and stored in the memory
- The number of nodes n_N is approximately equal to number of elements

A major part of the multigrid method is to compute the vector matrix product $\boldsymbol{Ku}$. The (assembled) global stiffness matrix is extremely sparse. On an isometric 3D grid, each node is connected to 27 nodes, which have three degrees of freedom. Hence, each row of the stiffness matrix contains a maximum of 81 entries. Considering three rows per node, the cost of a vector matrix product is equal to $81 \cdot 3n_N = 243n_N$ multiplications. If the assembled stiffness matrix is not available, the vector matrix product is computed on element level. The element stiffness matrix is full and has 576 entries. Hence, the number of scalar multiplications is approximately $576n_N$. However, the procedure is parallelizable.

The Jacobi method only requires computing the residual (vector matrix product) and inverting a diagonal matrix. Hence, the additional cost is $3nN$ multiplications.

In the lexicographic successive overrelaxation, a lower diagonal matrix is inverted. If the lower diagonal matrix $\boldsymbol{L}$ is available, solving the system of equations is trivial, leading to $41 \cdot 3n_N = 123n_N$ additional multiplications. However, this framework is strictly sequential and requires some indexing, leading to higher computational cost. If $\boldsymbol{L}$ is not available, the system of equations must be solved on element level. This means, sequentially for every node, the couplings to all neighbor nodes must be computed from the

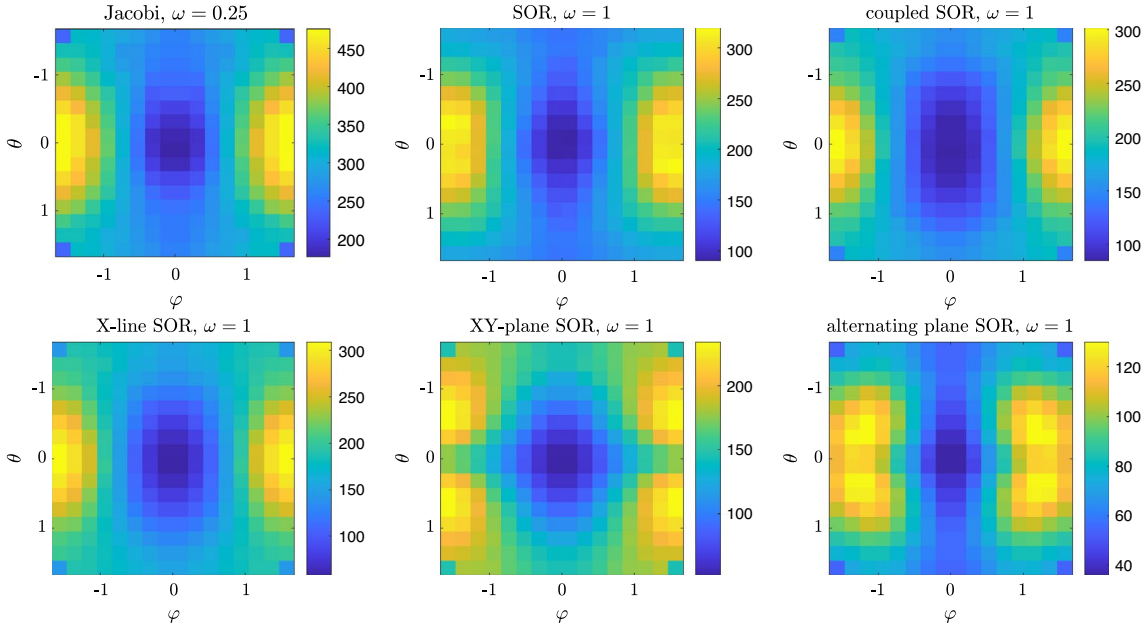

Fig. 22 Required number of iterations for the multigrid method to reach a relative tolerance of 10^{-10} for different constant material orientations φ, θ of Balsa wood. Here, the elasticity equations of the example problem 10b with optimized densities is solved using 4 grids. The colors indicate the required number of iterations

corresponding element stiffness matrices. The couplings are afterwards multiplied with the corresponding entries of the deformation vectors, leading to approximately $576n_N$ additional multiplications and a huge amount of indexing. The overall procedure again is fully sequential.

The remaining methods are based on a multicolor pattern and the inversion of a block diagonal matrix. In every sequence, the residual is computed for all degrees of freedom of the same color. Afterwards, the block-diagonal system of equations $\boldsymbol{D}_c^{-1}\left(\boldsymbol{f}_c - \boldsymbol{K}_{c,:}\begin{pmatrix}\boldsymbol{u}_{i+1,1\ldots c-1}\\ \boldsymbol{u}_{i,c\ldots n_c}\end{pmatrix}\right)$ is solved, leading to a state update. Using the updated state, the next sequence starts. Solving the system of equations with conjugate gradients and a tolerance of 10^{-2} requires approximately 5–10 iterations for the coupled SOR and 10–20 iterations for the line and plane smoothers. Each degree of freedom has contact with 3 (pointwise), 9 (line) or 27 (plane) other degrees of freedom, leading to a computational cost of 9 (pointwise), 27 (line) or 81 (plane) scalar multiplications per node and inner iteration. The overall framework is simply parallelized since the content of the sequences is parallelizable.

Besides the theoretical computational effort, data indexing, copying and other operations increase the computation time. However, highly efficient implementations might reach the theoretical results.

Iteration plots for topology optimized design and four grids

See Fig. 22.

Material properties of different orthotropic materials

In the following, typical material properties of different orthotropic materials are collected or computed.

Carbon fiber reinforced composites

For zero rotations and Voigt notation, the material compliance tensor $\boldsymbol{s}$ of transversal isotropic material reads

$$\boldsymbol{s} = \begin{pmatrix} \frac{1}{E_1} & -\frac{\nu_{12}}{E_1} & -\frac{\nu_{12}}{E_1} & 0 & 0 & 0 \\ -\frac{\nu_{12}}{E_1} & \frac{1}{E_2} & \frac{\nu_{23}}{E_2} & 0 & 0 & 0 \\ -\frac{\nu_{12}}{E_1} & \frac{\nu_{23}}{E_2} & \frac{1}{E_2} & 0 & 0 & 0 \\ 0 & 0 & 0 & \frac{1}{G_{12}} & 0 & 0 \\ 0 & 0 & 0 & 0 & \frac{1}{G_{12}} & 0 \\ 0 & 0 & 0 & 0 & 0 & \frac{1}{G_{23}} \end{pmatrix}. \tag{D3}$$

Typical values, which are used in the paper, are $E_1 = 140GPa, E_2 = 12GPa, G_{12} = 5.8GPa, G_{23} = 5.4GPa$, $\nu_{12} = 0.26$ and $\nu_{23} = 0.11$.

Balsa wood

The mechanical properties of Balsa wood are taken from Wang et al. (2019). For zero rotations and Nye notation, the material compliance tensor $\boldsymbol{s}$ reads

$$\boldsymbol{s} = \begin{pmatrix} \frac{1}{E_1} & -\frac{\nu_{12}}{E_1} & -\frac{\nu_{13}}{E_1} & 0 & 0 & 0 \\ -\frac{\nu_{12}}{E_1} & \frac{1}{E_2} & \frac{\nu_{23}}{E_2} & 0 & 0 & 0 \\ -\frac{\nu_{13}}{E_1} & \frac{\nu_{23}}{E_2} & \frac{1}{E_3} & 0 & 0 & 0 \\ 0 & 0 & 0 & \frac{1}{G_{12}} & 0 & 0 \\ 0 & 0 & 0 & 0 & \frac{1}{G_{12}} & 0 \\ 0 & 0 & 0 & 0 & 0 & \frac{1}{G_{23}} \end{pmatrix} \tag{D4}$$

with $E_1 = 6.3GPa$, $E_2 = 0.11GPa$, $E_3 = 0.3GPa$, $G_{12} = 0.2GPa, G_{13} = 0.31GPa, G_{23} = 0.03GPa, \nu_{12} = 0.49$, $\nu_{23} = 0.24$ and $\nu_{13} = 0.23$.

Acknowledgements Funded by the Deutsche Forschungsgemeinschaft (DFG, German Research Foundation)—508865334

Author contributions Jan Krüger: Conceptualization, Methodology, Software, Investigation, Writing original draft. Benedikt Kriegesmann: Review and Editing, Funding acquisition, Supervision.

Funding Open Access funding enabled and organized by Projekt DEAL.

Declarations

Conflict of interest The authors state that there is no Conflict of interest.

Replication of results The authors state that the paper contains all information necessary to reproduce the results. The underlying code will be made available at request.

Open Access This article is licensed under a Creative Commons Attribution 4.0 International License, which permits use, sharing, adaptation, distribution and reproduction in any medium or format, as long as you give appropriate credit to the original author(s) and the source, provide a link to the Creative Commons licence, and indicate if changes were made. The images or other third party material in this article are included in the article's Creative Commons licence, unless indicated otherwise in a credit line to the material. If material is not included in the article's Creative Commons licence and your intended use is not permitted by statutory regulation or exceeds the permitted use, you will need to obtain permission directly from the copyright holder. To view a copy of this licence, visit http://creativecommons.org/licenses/by/4.0/.

References

Aage N, Andreassen E, Lazarov BS (2015) Topology optimization using PETSc: an easy-to-use, fully parallel, open source topology optimization framework. Struct Multidisc Optim 51(3):565–572. https://doi.org/10.1007/s00158-014-1157-0

Aage N, Andreassen E, Lazarov BS, Sigmund O (2017) Giga-voxel computational morphogenesis for structural design. Nature 550(7674):84–86. https://doi.org/10.1038/nature23911

Amir O, Bendsøe MP, Sigmund O (2009) Approximate reanalysis in topology optimization. Int J Numer Meth Eng 78(12):1474–1491. https://doi.org/10.1002/nme.2536

Amir O, Sigmund O (2011) On reducing computational effort in topology optimization: how far can we go? Struct Multidisc Optim 44(1):25–29. https://doi.org/10.1007/s00158-010-0586-7

Amir O, Aage N, Lazarov BS (2014) On multigrid-CG for efficient topology optimization. Struct Multidisc Optim 49(5):815–829. https://doi.org/10.1007/s00158-013-1015-5

Arms RJ, Gates LD, Zondek B (1956) A method of block iteration. J Soc Ind Appl Math 4(4):220–229. https://doi.org/10.1137/0104012

Borrvall T, Petersson J (2001) Large-scale topology optimization in 3D using parallel computing. Comput Methods Appl Mech Eng 190(46):6201–6229. https://doi.org/10.1016/S0045-7825(01)00216-X

Briggs WL, Henson VE, McCormick SF (2000) A multigrid tutorial, 2nd edn. Society for Industrial and Applied Mathematics. https://doi.org/10.1137/1.9780898719505

Buhl T, Pedersen CBW, Sigmund O (2000) Stiffness design of geometrically nonlinear structures using topology optimization. Struct Multidisc Optim 19(2):93–104. https://doi.org/10.1007/s001580050089

Da Silva A, Kyriakides S (2007) Compressive response and failure of balsa wood. Int J Solids Struct 44(25):8685–8717. https://doi.org/10.1016/j.ijsolstr.2007.07.003

Davis TA (2006) Direct methods for sparse linear systems: fundamentals of algorithms. Society for Industrial and Applied Mathematics. https://doi.org/10.1137/1.9780898718881

Dreyer T, Maar B, Schulz V (2000) Multigrid optimization in applications. J Comput Appl Math 120(1):67–84. https://doi.org/10.1016/S0377-0427(00)00304-6

Evans DJ, Biggins MJ (1982) The solution of elliptic partial differential equations by a new block over-relaxation technique. Int J Comput Math 10(3–4):269–282. https://doi.org/10.1080/00207168208803287

Evgrafov A, Rupp CJ, Maute K, Dunn ML (2008) Large-scale parallel topology optimization using a dual-primal substructuring solver. Struct Multidisc Optim 36(4):329–345. https://doi.org/10.1007/s00158-007-0190-7

Ferguson WE Jr (1986) The rate of convergence of a class of block Jacobi schemes. SIAM J Numer Anal 23(2):297–303. https://doi.org/10.1137/0723021

Fulton SR, Ciesielski PE, Schubert WH (1986) Multigrid methods for elliptic problems: a review. Mon Weather Rev 114(5):943–959

Hammer VB, Olhoff N (2000) Topology optimization of continuum structures subjected to pressure loading. Struct Multidisc Optim 19(2):85–92. https://doi.org/10.1007/s001580050088

Herrero-Pérez D, Martínez Castejón PJ (2021) Multi-GPU acceleration of large-scale density-based topology optimization. Adv Eng Softw 157–158:103006. https://doi.org/10.1016/j.advengsoft.2021.103006

Hestenes MR, Stiefel E (1952) Methods of conjugate gradients for solving linear systems. J Res Natl Bur Stand 49(6):2379

Jantos DR, Hackl K, Junker P (2020) Topology optimization with anisotropic materials, including a filter to smooth fiber pathways. Struct Multidisc Optim 61(5):2135–2154. https://doi.org/10.1007/s00158-019-02461-x. (**Accessed 2020-06-28**)

Kipping J, Schüppstuhl T (2023) Load-oriented nonplanar additive manufacturing method for optimized continuous carbon fiber parts. Materials 16(3):998. https://doi.org/10.3390/ma16030998

Lazarov BS, Sigmund O (2011) Filters in topology optimization based on Helmholtz-type differential equations. Int J Numer Meth Eng 86(6):765–781. https://doi.org/10.1002/nme.3072

Lee J, Kim D, Nomura T, Dede EM, Yoo J (2018) Topology optimization for continuous and discrete orientation design of functionally graded fiber-reinforced composite structures. Compos Struct 201:217–233. https://doi.org/10.1016/j.compstruct.2018.06.020

Liu H, Hu Y, Zhu B, Matusik W, Sifakis E (2018) Narrow-band topology optimization on a sparsely populated grid. ACM Trans Graph 37(6):251–125114. https://doi.org/10.1145/3272127.3275012

Lund E (2017) Discrete material and thickness optimization of laminated composite structures including failure criteria. Struct Multidisc Optim. https://doi.org/10.1007/s00158-017-1866-2

Luo S, Yang F, Wang Y (2024) An efficient isogeometric topology optimization based on the adaptive damped geometric multigrid method. Adv Eng Softw 196:103712. https://doi.org/10.1016/j.advengsoft.2024.103712

Ma J, Li Z, Zhao Z-L, Xie YM (2021) Creating novel furniture through topology optimization and advanced manufacturing. Rapid Prototyp J 27(9):1749–1758. https://doi.org/10.1108/RPJ-03-2021-0047

Mahdavi A, Balaji R, Frecker M, Mockensturm EM (2006) Topology optimization of 2D continua for minimum compliance using parallel computing. Struct Multidisc Optim 32(2):121–132. https://doi.org/10.1007/s00158-006-0006-1

Montemurro M, Mas A, Zerrouq S-E (2024) Topology and anisotropy optimisation of continua using non-uniform rational basis spline entities. Comput Methods Appl Mech Eng 420:116714. https://doi.org/10.1016/j.cma.2023.116714

Morano E, Mavriplis DJ, Venkatakrishnan V (1998) Coarsening strategies for unstructured multigrid techniques with application to anisotropic problems. SIAM J Sci Comput 20(2):393–415. https://doi.org/10.1137/S1064827595287638

Oosterlee CW (1997) A GMRES-based plane smoother in multigrid to solve 3D anisotropic fluid flow problems. J Comput Phys 130(1):41–53. https://doi.org/10.1006/jcph.1996.5442

Padhi AP, Chakraborty S, Chakrabarti A, Chowdhury R (2023) Efficient hybrid topology optimization using GPU and homogenization-based multigrid approach. Eng Comput 39(5):3593–3615. https://doi.org/10.1007/s00366-022-01771-x

Peetz D, Elbanna A (2021) On the use of multigrid preconditioners for topology optimization. Struct Multidisc Optim 63(2):835–853. https://doi.org/10.1007/s00158-020-02750-w

Saad Y, Schultz MH (1986) GMRES: a generalized minimal residual algorithm for solving nonsymmetric linear systems. SIAM J Sci Stat Comput 7(3):856–869. https://doi.org/10.1137/0907058

Schmidt M-P, Couret L, Gout C, Pedersen CBW (2020) Structural topology optimization with smoothly varying fiber orientations. Struct Multidisc Optim 62(6):3105–3126. https://doi.org/10.1007/s00158-020-02657-6

Shaidurov VV (1995) Multigrid methods for finite elements. Springer, Dordrecht. https://doi.org/10.1007/978-94-015-8527-9

Sigmund O (2007) Morphology-based black and white filters for topology optimization. Struct Multidisc Optim 33(4–5):401–424. https://doi.org/10.1007/s00158-006-0087-x

Steltner K, Kipping J, Kriegesmann B, Schüppstuhl T (2025) A workflow for designing stiffness-optimized structures in the context of additive manufacturing of endless fiber-reinforced composites, Journal of Thermoplast Composite Materials. https://doi.org/10.1177/08927057251332788

Stüben K, Trottenberg U (1982) Multigrid methods: fundamental algorithms, model problem analysis and applications. In: Hackbusch W, Trottenberg U (eds) Multigrid methods. Lecture Notes in Mathematics. Springer, Berlin, pp 1–176. https://doi.org/10.1007/BFb0069928

Svanberg K (1987) The method of moving asymptotes—a new method for structural optimization. Int J Numer Meth Eng 24(2):359–373. https://doi.org/10.1002/nme.1620240207

Thibaut B, Gril J, Fournier M (2001) Mechanics of wood and trees: some new highlights for an old story. Comptes Rendus de l'Académie des Sciences—Series IIB—Mechanics 329(9):701–716. https://doi.org/10.1016/S1620-7742(01)01380-0

Thole C-A, Trottenberg U (1986) Basic smoothing procedures for the multigrid treatment of elliptic 3D operators. Appl Math Comput 19(1):333–345. https://doi.org/10.1016/0096-3003(86)90112-8

Träff EA, Sigmund O, Aage N (2021) Topology optimization of ultra high resolution shell structures. Thin-Walled Struct 160:107349. https://doi.org/10.1016/j.tws.2020.107349

Trottenberg U, Oosterlee CW, Schüller A, Brandt A, Oswald P, Stüben K (2007) Multigrid. Transferred to digital print edn. Elsevier Academic Press, Amsterdam Heidelberg

Vito AF, Vicente WM, Xie YM (2023) Topology optimization applied to the core of structural engineered wood product. Structures 48:1567–1575. https://doi.org/10.1016/j.istruc.2023.01.036

Wallin M, Ivarsson N, Amir O, Tortorelli D (2020) Consistent boundary conditions for PDE filter regularization in topology optimization. Struct Multidisc Optim. https://doi.org/10.1007/s00158-020-02556-w

Wang S, Sturler ED, Paulino GH (2007) Large-scale topology optimization using preconditioned Krylov subspace methods with recycling. Int J Numer Meth Eng 69(12):2441–2468. https://doi.org/10.1002/nme.1798

Wang Z, Wang Y, Cao Y, Gao Z (2019) Measurements of the shear modulus of materials by the free-plate torsional mode shape method. J Test Eval 47(2):1163–1181. https://doi.org/10.1520/JTE20160471

Wesseling P (1992) An introduction to multigrid methods. John Wiley & Sons Ltd, Chichester

Wienands R, Joppich W (2004) Practical Fourier analysis for multigrid methods. Chapman and Hall/CRC, New York. https://doi.org/10.1201/9781420034998

Wu J, Dick C, Westermann R (2016) A system for high-resolution topology optimization. IEEE Trans Visual Comput Graphics 22(3):1195–1208. https://doi.org/10.1109/TVCG.2015.2502588

Publisher's Note Springer Nature remains neutral with regard to jurisdictional claims in published maps and institutional affiliations.